Joint Beamforming and Reflecting Design for IRS-aided Wireless Powered Over-the-Air Computation and Communication Networks

Sun Mao, Ning Zhang, *Senior Member, IEEE*, Lei Liu, Tang Liu, Jie Hu, *Senior Member, IEEE*, Kun Yang, *Fellow, IEEE*, and Dusit Niyato, *Fellow, IEEE*

***Abstract*—To satisfy the heterogeneous service requirements in future internet of things (IoT), this paper investigates the novel framework for intelligent reflecting surface (IRS)-aided wireless powered over-the-air computation (AirComp) and communication networks, where the IoT devices first harvest energy from the downlink signal sent by the base station, and then conduct the information transmissions and AirComp in the uplink. In particular, the IRS is used to improve the efficiency of wireless energy transfer, and alleviate the harmful interference between the communication and AirComp signals. To balance the performance of such an integrated system, we present two joint beamforming and reflection optimization problems via minimizing the computation distortion and maximizing the sum rate, respectively. To solve the non-convex problems, we develop the alternating optimization framework with proved convergence, in which the penalty function-based method and variable substitution technique are exploited to acquire the optimal solutions of beamformers and reflection parameters. Finally, simulation results show that the proposed method realizes significantly higher computation accuracy and communication rate, in comparison with several existing benchmark methods.**

***Index Terms*—Intelligent reflecting surface, over-the-air computation, non-orthogonal multiple access, wireless energy transfer, Internet of Things.**

I. Introduction

The recent advancement of IoT leads to the explosive growth in terminal devices. It is expected that over 29.4 billion IoT devices will be installed in 2030 to execute some environment sensing tasks and to enable multitudinous applications, e.g., smart cities, industrial automation and emergency rescue [1]. Typically, these applications require stable energy supply and high-speed communications. Radio-frequency-based wireless energy transfer (WET) is developed to offer convenient, controllable and stable energy supply for massive IoT devices, in which the base station (BS) can broadcast downlink energy signals to charge distributed IoT devices [2], [3]. Nowadays, the efficiency of WET has been significantly enhanced with the development of hardwares and algorithms. For instance, Xiaomi company has proposed "Mi Air Charge", which can deliver up to 5 watt power over the wireless channels to multiple IoT devices simultaneously within a distance of several meters [4].

Furthermore, due to the limited spectrum resources, conventional orthogonal multiple access method cannot ensure the high-speed communications for massive IoT devices. Non-orthogonal multiple access (NOMA) is thus proposed to enable massive access of ubiquitous IoT devices [5], [6]. Nevertheless, the severe co-channel interference restricts the application of NOMA in IoT [7], [8]. To tackle this issue, spatial beamforming is recognized as a promising solution, where BS and IoT devices are equipped with multiple antennas for conducting the refined transmit/reflect beamforming to reduce the harmful co-channel interference in NOMA-based IoT [9].

In addition to the energy supply and data transmissions, the real-time data processing/computation is another challenge faced by IoT [10]–[12]. For instance, in the temperature measurement applications, the BS prefers to obtain the average temperature measured by multiple IoT devices, instead of acquiring the individual measured data. However, the conventional *transmit-then-compute* approach requires two phases to achieve the data computation, and it will be low-efficiency and high-latency. To this end, AirComp is developed to support the direct computation of distributed data from IoT devices, through utilizing the superposition property of wireless transmission channels [13]–[15]. Despite the benefits introduced by AirComp, it also incurs the deviation between the desired computation result and the actual computation result [16]. In [17], Cao *et al.* studied the interference management scheme to minimize the computation error for multi-cell AirComp systems. In [18], Fu *et al.* utilized the mobility of UAV to reduce the computation error of AirComp systems.

To satisfy the heterogeneous service requirements in IoT, it is meaningful and essential to design the integrated framework of energy transfer, data communication and AirComp, which will lead to a new design paradigm, i.e., wireless powered

This work is supported in part by the Natural Science Foundation of China under Grants 62241108, 62132004, 61971102 and 62072320, in part by the Natural Science Foundation of Sichuan Province under Grants 2022NSFSC0479 and 2022NSFSC0569, in part by the Sichuan Science and Technology Program under Grants 2022YFH0022 and 22QYCX0168.

S. Mao and Tang Liu are with the College of Computer Science, Sichuan Normal University, Chengdu, 610101, China, and also with Visual Computing and Virtual Reality Key Laboratory of Sichuan, Sichuan Normal University, Chengdu, 610101, China. (e-mail: sunmao@sicnu.edu.cn; liutang@sicnu.edu.cn).

N. Zhang is with the Department of Electrical and Computer Engineering, University of Windsor, ON, N9B 3P4, Canada (e-mail: ning.zhang@ieee.org).

Lei Liu is with the Guangzhou Institute of Technology, Xidian University, Guangzhou 510555, China, and the Shanxi Key Laboratory of Information Communication Network and Security, Xi'an University of Posts and Telecommunications, Xi'an, Shanxi 710121, China. (e-mail: tianjiaoliulei@163.com).

J. Hu is with the School of Information and Communication Engineering, University of Electronic Science and Technology of China, Chengdu, 611731, China. (e-mail: hujie@uestc.edu.cn).

Kun Yang is with the School of Computer Science and Electronic Engineering, University of Essex, Colchester, CO4 3SQ, U.K. (e-mail: kunyang@essex.ac.uk).

D. Niyato is with School of Computer Science and Engineering, Nanyang Technological University, 639798, Singapore (e-mail: dniyato@ntu.edu.sg).

AirComp and communication networks. In [19], Li *at al.* proposed the power allocation and beamforming optimization strategy for wireless powered AirComp systems. In [20], Qi *et al.* focused on the joint transmit and receive beamforming scheme for an integrated multi-antenna AirComp and communication network. In [21], the same group extended their work to wireless powered AirComp and communication networks, where IoT devices need to harvest radio-frequency energy to conduct the uplink information transmissions and AirComp. Although performance advantages of the wireless powered AirComp and communication network, it is fundamentally restricted by uncontrollable wireless transmission environments and the nonnegligible co-channel interference between communication and computation signals.

Benefited from the advantage of reconstructing the wireless channels, IRS has attracted extensive attentions from both industrial and academia [22]–[25]. IRS is composed of a large number of passive/active reflection elements, where the phase/amplitude of incident signals can be dynamically adjusted to form refined reflect beamforming to enhance the intended signal and to eliminate the harmful interference signal at receivers. Therefore, the IRS is of great potential in improving the efficiency of wireless powered AirComp and communication networks. In [26]–[33], the authors utilized the IRS technique to improve the performance of sum rate, power consumption, energy efficiency, security, latency, etc., for wireless energy and information transfer systems. In [34]–[37], Fang *et al.* aimed at minimizing the computation error for IRS-aided AirComp systems. In [38], Wang *et al.* focused on the optimal beamforming strategy for IRS-assisted wireless powered AirComp systems. Nevertheless, only uplink AirComp was considered in this article, and it cannot reveal the tradeoff relationship between uplink information transmission and AirComp. Table I compares this article with existing literature.

As observed in Table I, the transmit and receive beamforming was investigated to improve the efficiency of wireless energy transfer, information communication or AirComp in [19]–[21]. Moreover, IRS was utilized to enhance the efficiency of wireless energy/information transmissions [26]–[33], and to reduce the computation error [34]–[38] of AirComp. However, the integration framework of IRS-aided wireless powered AirComp and communication networks was not investigated in existing literature. Moreover, the joint beamforming and reflecting optimization method was not developed to balance the heterogeneous performance requirements of such an integrated network. Notice that the joint optimization problem is extremely challenging considering complex coupled relationship between energy transfer, information transmissions and AirComp. As expected, available energy of IoT devices for AirComp and information transmissions is restricted by the harvested radio-frequency energy in the downlink. Besides, the co-channel interference originated from AirComp will degrade the signal-to-interference-plus-noise-ratio (SINR) of information transmissions, and the computation error can be deteriorated due to the existence of information transmissions. Meanwhile, despite the benefits introduced by the IRS, it is difficult to configure the reflection parameters to coordinate with transmit/receive beamforming for improving the performance of such an integrated system. Due to the highly coupled multi-dimensional optimization variables and diverse performance requirements, the existing beamforming methods cannot be exploited in IRS-aided wireless powered AirComp and communication networks. As a result, there is an urgent requirement to design new optimization framework and algorithms for IRS-aided wireless powered AirComp and communication networks.

This paper considers a typical IRS-aided wireless powered AirComp and communication network, where each IoT device first harvests the radio-frequency energy from the BS, and then conducts the uplink information transmission and AirComp simultaneously. The contribution of this article is summarized as follows.

- A Novel framework is proposed for balancing the communication rate and computation accuracy of IRS-assisted wireless powered AirComp and communication networks. In particular, each IoT device and BS dedicate two transmit and receive beamformers separately for uplink information transmissions and AirComp, while the IRS reflect coefficient is configured to reduce the harmful co-channel interference between communication and AirComp.
- A new optimization problem is formulated to minimize the computation MSE under the energy causality restrictions and communication SINR constraints, with the joint optimization of the transmit beamforming at IoT devices, reflection matrix of the IRS, energy beamforming and receive beamforming of the BS. To solve the non-convex problem, we develop an alternating optimization framework to sequentially optimize the receive, reflect and transmit beamfomers, where the variable substitution technique and penalty function-based method are utilized to solve each subproblem.
- We further present the sum rate maximization problem under the computation MSE and energy causality constraints, via jointly optimizing the transmit and receive beamforming, as well as the reflection matrix of IRS. We first adopt an approximate method to rewrite the non-concave sum rate expression to a tractable form. Then, an alternating optimization method is developed to decouple the optimization variables, and the variable substitution technique and penalty function-based method are applied to acquire the optimal solutions of beamformers and reflection parameters.

Simulation results show that the optimal configuration of IRS contributes significantly to improving the communication and computation performance of considered systems, especially when there are a large number of transmit antennas and reflection elements. Besides, the integrated design can achieve comparable communication rate and computation accuracy than *Communication only* scheme and *Computation only* scheme, respectively.

The remainder of this article is outlined as follows. Section II introduces the system model for IRS-aided wireless powered AirComp and communication networks. Sections

TABLE I: Synopsis of relevant research works

Ref.	Optimization target	IRS	AirComp	WET	Communication
[19]	Computation MSE	✗	✓	Linear energy harvesting	✓
[20]	Computation MSE&Sum rate	✗	✓	✗	✓
[21]	Computation MSE	✗	✓	Linear energy harvesting	✓
[26], [27]	Sum rate	✓	✗	Linear energy harvesting	✓
[28], [29]	System power consumption	✓	✗	Linear energy harvesting	✓
[30]	Common throughput	✓	✗	Linear energy harvesting	✓
[31]	Secrecy throughput	✓	✗	Linear energy harvesting	✓
[32]	Energy efficiency	✓	✗	Linear energy harvesting	✓
[33]	Total transmission time	✓	✗	Linear energy harvesting	✓
[34]–[37]	Computation MSE	✓	✓	✗	✗
[38]	Computation MSE	✓	✓	Linear energy harvesting	✗
This article	Computation MSE&Sum rate	✓	✓	Linear&Non-Linear energy harvesting	✓

III and IV investigate the joint beamforming and reflection optimization methods for minimizing the MSE and maximizing the sum rate, respectively. Section V extends the joint beamforming and reflect optimization method to the scenario with non-linear energy harvesting model. Simulation results are presented in Section VI. We conclude this paper in Section VII.

II. System Model

As shown in Fig. 1, this paper considers an IRS-aided wireless powered AirComp and communication network, which includes a BS with N_A antennas, an IRS with M reflection elements, K IoT devices with N_I antennas. We denote the sets of IRS's reflection elements and IoT devices as $\mathcal{M} = \{1, 2, \cdots, M\}$ and $\mathcal{K} = \{1, 2, \cdots, K\}$, respectively. The time-division duplex is utilized to coordinate the downlink wireless energy transfer, uplink AirComp and information transmissions.

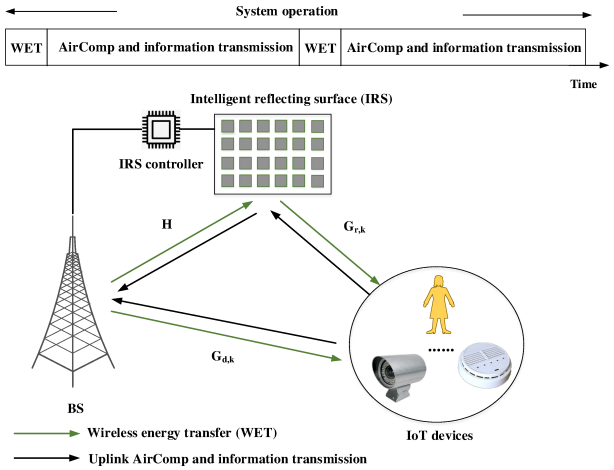

Fig. 1: IRS-aided wireless powered AirComp and communication networks.

In the first half of the time slot, the BS broadcasts the downlink energy signals to charge IoT devices with the aid of IRS. According to classic energy harvesting model in [21], the energy collected by the k-th IoT device is expressed as

$$E_k = T_{ET}\eta_k \|\mathbf{G}_{E,k}^H \mathbf{v}\|^2, \forall k \in \mathcal{K}, \quad (1)$$

where T_{ET} indicates the duration for downlink energy transfer, $\eta_k \in [0, 1]$ represents the energy conversion efficiency of the k-th IoT device, $\mathbf{G}_{E,k}^H = \mathbf{G}_{d,k}^H + \mathbf{G}_{r,k}^H \Theta_E \mathbf{H}$, where $\mathbf{G}_{d,k} \in \mathbb{C}^{N_A \times N_I}$, $\mathbf{G}_{r,k} \in \mathbb{C}^{M \times N_I}$ and $\mathbf{H} \in \mathbb{C}^{M \times N_A}$ stands for the channels between the BS and the k-th IoT device, between the IRS and the k-th IoT device, and between the BS and the IRS, respectively, $\mathbf{v} \in \mathbb{C}^{N_A \times 1}$ denotes the energy beamformer at the BS, $\Theta_E = \text{diag}\{e^{j\theta_{E,1}}, e^{j\theta_{E,2}}, \cdots, e^{j\theta_{E,M}}\}$ is the IRS reflection matrix for downlink energy transfer, where $\theta_{E,m} \in (0, 2\pi]$ indicates the phase shift of m-th reflection element. Noted that the power harvested from noise is generally negligible, when compared to the power harvested from the radio-frequency signal [39]. In order to unless the potential of IRS, it is assumed that the BS can obtain accurate channel state information (CSI) in considered systems [40]. In practice, the CSI of direct channels can be estimated via conventional methods by setting IRS into absorbing mode. In addition, a small number of low-power sensors can be installed at the IRS for estimating the CSI of channels between the IRS and BS/IoT devices.

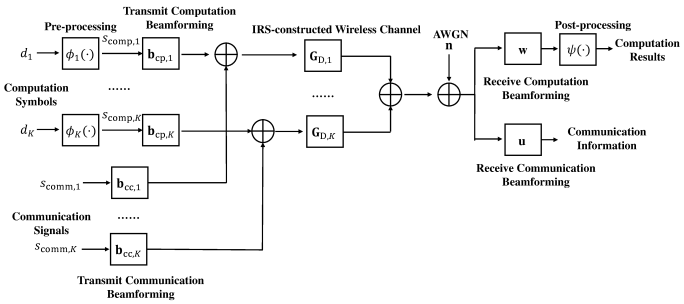

Fig. 2: The system framework of uplink signal transmission and reception.

In the second half of the time slot, the IoT devices will utilize the harvested energy to execute two tasks in the uplink, namely AirComp and information transmissions. Hence, the transmit signals of IoT devices include two parts, one for information transmissions and the other for data computation using the AirComp technique. For convenience, the former signal and the latter signal are denoted by communication signal and computation signal, respectively. As seen in Fig. 2, each IoT device first conducts transmit beamforming for the communication signal and computation signal, and then sends

the superposed signal to the BS. Benefited from the advantage of AirComp, the BS will utilize the receive computation beamforming to obtain the computation result directly. Besides, the communication information can be decoded by the BS through exploiting the receive communication beamforming.

TABLE II: Some examples of nomographic functions

Function	ϕ_k	ψ	f
Arithmetic Mean	$\phi_k = d_k$	$\psi = \frac{1}{K}$	$f = \frac{1}{K}\sum_{k=1}^{K} d_k$
Geometric Mean	$\phi_k = \ln(d_k)$	$\psi = \exp(\frac{\cdot}{K})$	$f = (\prod_{k=1}^{K} d_k)^{1/K}$
Polynomial	$\phi_k = \nu_k d_k^{\varrho_k}$	$\psi = 1$	$f = \sum_{k=1}^{K} \nu_k d_k^{\varrho_k}$
Euclidean Norm	$\phi_k = d_k^2$	$\psi = \sqrt{\cdot}$	$f = \sqrt{\sum_{k=1}^{K} d_k^2}$

Furthermore, we denote d_k and $s_{\text{comm},k}$ as the computation symbol and communication signal of k-th IoT device, respectively. Based on the principle of AirComp, the BS tends to acquire the the desired nomographic function of computation symbols from all IoT devices, instead of obtaining the individual computation symbol of each IoT device. Defining f as the target function at the BS, it follows that

$$f = \psi\left(\sum_{k=1}^{K} \phi_k(d_k)\right), \tag{2}$$

where ϕ_k and ψ denote the pre-processing function at the k-th IoT device and post-processing function at the BS, respectively. Besides, $s_{\text{comp},k} = \phi_k(d_k)$ is defined as the computation signal at the k-th IoT device, which satisfies $\mathbb{E}(s_{\text{comp},k}) = 0$, $\mathbb{E}(s_{\text{comp},k}(s_{\text{comp},k})^H) = 1$ and $\mathbb{E}(s_{\text{comp},k}(s_{\text{comp},j})^H) = 0$ for $k \neq j$. Note that this article focuses on a scenario that the BS wants to acquire the desired function $f = \sum_{k=1}^{K} s_{\text{comp},k}$ [38]. In addition, the other nomographic functions can also be computed by designing proper pre-processing and post-processing functions (See examples in TABLE II). According to above descriptions, the transmit signal of the k-th IoT device is given by

$$\mathbf{x}_k = \mathbf{b}_{\text{cp},k} s_{\text{comp},k} + \mathbf{b}_{\text{cc},k} s_{\text{comm},k}, \forall k \in \mathcal{K}, \tag{3}$$

where $\mathbf{b}_{\text{cp},k} \in \mathbb{C}^{N_I \times 1}$ and $\mathbf{b}_{\text{cc},k} \in \mathbb{C}^{N_I \times 1}$ represent the transmit beamformers of computation signal and communication signal at the k-th IoT device, respectively. Defining $Q_{\text{ini},k}$ as the initial battery energy of k-th IoT device, its transmit power is restricted by the sum of initial energy and harvested energy, which yields that

$$\|\mathbf{b}_{\text{cp},k}\|^2 + \|\mathbf{b}_{\text{cc},k}\|^2 \leq \frac{E_k + Q_{\text{ini},k}}{T_{IT}}, \forall k \in \mathcal{K}. \tag{4}$$

where T_{IT} represents the time duration for uplink information transmissions and AirComp.

Furthermore, the received signal of the BS is denoted by

$$\mathbf{y} = \sum_{k=1}^{K} \mathbf{G}_{D,k}\mathbf{x}_k + \mathbf{n}. \tag{5}$$

Note that $\mathbf{n} \in \mathcal{CN}(0, \delta^2\mathbf{I})$ indicates the additive white Gaussian noise, $\mathbf{G}_{D,k} = \mathbf{G}_{d,k} + \mathbf{H}^H\Theta_D\mathbf{G}_{r,k}$, and $\Theta_D = \text{diag}\{e^{j\theta_{D,1}}, e^{j\theta_{D,2}}, \cdots, e^{j\theta_{D,M}}\}$ is the IRS reflection matrix for uplink signal transmissions, where $\theta_{D,m} \in (0, 2\pi]$ indicates the phase shift of m-th reflection element. As shown in Fig. 2, the BS will utilize the receive computation beamformer $\mathbf{w} \in \mathbb{C}^{N_A \times 1}$ to recover the desired function f after receiving the superposition signals from all IoT devices. Hence, the estimated function $\hat{f}$ at the BS is written as

$$\begin{aligned}\hat{f} = &\mathbf{w}^H \sum_{k=1}^{K} \mathbf{G}_{D,k}\mathbf{b}_{\text{cp},k} s_{\text{comp},k} + \\ &\mathbf{w}^H \sum_{k=1}^{K} \mathbf{G}_{D,k}\mathbf{b}_{\text{cc},k} s_{\text{comm},k} + \mathbf{w}^H\mathbf{n}.\end{aligned} \tag{6}$$

Generally, the computation error is evaluated by the MSE between the target function f and the estimated function $\hat{f}$, which follows that

$$\begin{aligned}&\text{MSE}(f, \hat{f}) = \mathbb{E}\left[|f - \hat{f}|^2\right] = \\ &\sum_{k=1}^{K} |\mathbf{w}^H\mathbf{G}_{D,k}\mathbf{b}_{\text{cp},k} - 1|^2 + \sum_{k=1}^{K} |\mathbf{w}^H\mathbf{G}_{D,k}\mathbf{b}_{\text{cc},k}|^2 + \delta^2\|\mathbf{w}\|^2.\end{aligned} \tag{7}$$

Next, we will discuss the processing of communication signals at the BS. Let us denote $\mathbf{u} \in \mathbb{C}^{N_A \times 1}$ as the receive beamforming vector for recovering the communication signals at the BS. Therefore, the received signal for decoding the communication information is expressed as

$$\begin{aligned}y = &\mathbf{u}^H \sum_{k=1}^{K} \mathbf{G}_{D,k}\mathbf{b}_{\text{cp},k} s_{\text{comp},k} + \\ &\mathbf{u}^H \sum_{k=1}^{K} \mathbf{G}_{D,k}\mathbf{b}_{\text{cc},k} s_{\text{comm},k} + \mathbf{u}^H\mathbf{n}.\end{aligned} \tag{8}$$

Since the signals decoded before the k-th IoT device's signal have been subtracted from y, so the SINR for decoding the information of the k-th IoT device is written as

$$\begin{aligned}&\Gamma_k = \frac{|\mathbf{u}^H\mathbf{G}_{D,k}\mathbf{b}_{\text{cc},k}|^2}{\sum_{i=k+1}^{K} |\mathbf{u}^H\mathbf{G}_{D,k}\mathbf{b}_{\text{cc},i}|^2 + \sum_{i=1}^{K} |\mathbf{u}^H\mathbf{G}_{D,k}\mathbf{b}_{\text{cp},i}|^2 + \delta^2\|\mathbf{u}\|^2}, \\ &\forall k \in \mathcal{K}.\end{aligned} \tag{9}$$

In this paper, the computation and communication performance are evaluated by the MSE of computation result and the sum rate of information transmissions, respectively. As observed in (7) and (9), the system performance depends on the transmit beamformers $\{\mathbf{b}_{\text{cc},k}, \mathbf{b}_{\text{cp},k}\}$ of IoT devices, reflection matrix $\{\Theta_E, \Theta_D\}$ of IRS, energy beamformer $\mathbf{v}$ and receive beamformers $\{\mathbf{u}, \mathbf{w}\}$ of BS. In the following Sections III and IV, we will jointly optimize the beamforming and reflection strategies via minimizing the MSE and maximizing the sum rate, respectively.

III. MSE MINIMIZATION PROBLEM

This section aims at minimizing the MSE of computation result, while ensuring the minimum SINR requirements of

information transmissions, which is formulated as

$$\begin{aligned}\min_{\substack{\{\mathbf{v},\mathbf{u},\mathbf{w},\mathbf{b}_{\text{cc},k},\\ \mathbf{b}_{\text{cp},k},\Theta_E,\Theta_D\}}} \quad & \text{MSE}(f,\hat{f})\\ \text{s.t.} \quad & \text{C1: } \Gamma_k \geq r_{\min,k}, \forall k \in \mathcal{K},\\ & \text{C2: } \|\mathbf{b}_{\text{cp},k}\|^2 + \|\mathbf{b}_{\text{cc},k}\|^2 \leq \\ & \frac{Q_{\text{ini},k} + T_{ET}\eta_k \|\mathbf{G}_{E,k}^H \mathbf{v}\|^2}{T_{IT}}, \forall k \in \mathcal{K},\\ & \text{C3: } 0 \leq \theta_{E,m} \leq 2\pi, \forall m \in \mathcal{M},\\ & \text{C4: } 0 \leq \theta_{D,m} \leq 2\pi, \forall m \in \mathcal{M},\\ & \text{C5: } \|\mathbf{v}\|^2 \leq P_{\max,A},\end{aligned} \tag{10}$$

where $P_{\max,A}$ represents the maximum transmit power at the BS. In (10), C1 restricts the minimum SINR requirements of IoT devices, C2 indicates the energy causality constraints of IoT devices, C3-C4 denotes the phase shift constraints of reflection elements at the IRS, and C5 represents the maximum transmit power constraint of the BS.

Because of the non-convex MSE expression and the highly coupled optimization variables, the optimal solution of non-convex problem (10) cannot be acquired via standard methods in polynomial time. Based on the block coordinate descent (BCD) method, this paper decouples the optimization variables into three subproblems, namely energy and receive beamforming optimization subproblem, phase shift optimization subproblem, and transmit beamforming optimization subproblem. The details for solving the three subproblems are elaborated in the following subsections.

A. Energy and Receive Beamforming Optimization Subproblem

Under given $\{\mathbf{b}_{\text{cc},k}^*, \mathbf{b}_{\text{cp},k}^*, \Theta_E^*, \Theta_D^*\}$, (10) is reduced as

$$\min_{\{\mathbf{v},\mathbf{u},\mathbf{w}\}} \sum_{k=1}^{K} |\mathbf{w}^H \mathbf{G}_{D,k}^* \mathbf{b}_{\text{cp},k}^* - 1|^2 + \sum_{k=1}^{K} |\mathbf{w}^H \mathbf{G}_{D,k}^* \mathbf{b}_{\text{cc},k}^*|^2 + \delta^2 \|\mathbf{w}\|^2 \tag{11a}$$

$$\text{s.t.} \quad \frac{|\mathbf{u}^H \mathbf{G}_{D,k}^* \mathbf{b}_{\text{cc},k}^*|^2}{\sum_{i=k+1}^{K} |\mathbf{u}^H \mathbf{G}_{D,k}^* \mathbf{b}_{\text{cc},i}^*|^2 + \sum_{i=1}^{K} |\mathbf{u}^H \mathbf{G}_{D,k}^* \mathbf{b}_{\text{cp},i}^*|^2 + \delta^2 \|\mathbf{u}\|^2} \geq r_{\min,k}, \forall k \in \mathcal{K}, \tag{11b}$$

$$\|\mathbf{b}_{\text{cp},k}^*\|^2 + \|\mathbf{b}_{\text{cc},k}^*\|^2 \leq \frac{T_{ET}\eta_k \|(\mathbf{G}_{E,k}^*)^H \mathbf{v}\|^2}{T_{IT}} + \frac{Q_{\text{ini},k}}{T_{IT}}, \forall k \in \mathcal{K}, \tag{11c}$$

$$\|\mathbf{v}\|^2 \leq P_{\max,A}, \tag{11d}$$

where $\mathbf{G}_{D,k}^* = \mathbf{G}_{d,k} + \mathbf{H}^H \Theta_D^* \mathbf{G}_{r,k}$ and $(\mathbf{G}_{E,k}^*)^H = \mathbf{G}_{d,k}^H + \mathbf{G}_{r,k}^H \Theta_E^* \mathbf{H}$. Next, we first infer the optimal $\mathbf{w}$ in *Theorem 1*, and then adopt the variable substitution technique and penalty function-based algorithm to obtain the optimal $\{\mathbf{u}, \mathbf{v}\}$.

Theorem 1: The optimal receive computation beamforming $\mathbf{w}$ is expressed as

$$\mathbf{w}^* = (\sum_{k=1}^{K} (\mathbf{G}_{D,k}^* \mathbf{b}_{\text{cp},k}^* (\mathbf{b}_{\text{cp},k}^*)^H (\mathbf{G}_{D,k}^*)^H + \mathbf{G}_{D,k}^* \mathbf{b}_{\text{cc},k}^* (\mathbf{b}_{\text{cc},k}^*)^H (\mathbf{G}_{D,k}^*)^H) + \delta^2 \mathbf{I})^{-1} \sum_{k=1}^{K} \mathbf{G}_{D,k}^* \mathbf{b}_{\text{cp},k}^*. \tag{12}$$

Proof: Let us define $\text{MSE}(\mathbf{w}) = \sum_{k=1}^{K} |\mathbf{w}^H \mathbf{G}_{D,k}^* \mathbf{b}_{\text{cp},k}^* - 1|^2 + \sum_{k=1}^{K} |\mathbf{w}^H \mathbf{G}_{D,k}^* \mathbf{b}_{\text{cc},k}^*|^2 + \delta^2 \|\mathbf{w}\|^2$. The optimal $\mathbf{w}$ is obtained at the stationary point of $\text{MSE}(\mathbf{w})$. The first-order derivation of $\text{MSE}(\mathbf{w})$ is given by

$$\frac{\partial \text{MSE}(\mathbf{w})}{\partial \mathbf{w}} = 2(\sum_{k=1}^{K} (\mathbf{G}_{D,k}^* \mathbf{b}_{\text{cp},k}^* (\mathbf{b}_{\text{cp},k}^*)^H (\mathbf{G}_{D,k}^*)^H \mathbf{w} + \mathbf{G}_{D,k}^* \mathbf{b}_{\text{cc},k}^* (\mathbf{b}_{\text{cc},k}^*)^H (\mathbf{G}_{D,k}^*)^H \mathbf{w} - \mathbf{G}_{D,k}^* \mathbf{b}_{\text{cp},k}^*) + \delta^2 \mathbf{w}) \tag{13}$$

By setting $\frac{\partial \text{MSE}(\mathbf{w})}{\partial \mathbf{w}} = 0$, the optimal $\mathbf{w}^*$ is acquired as given in (12). ■

As observed, the optimal $\mathbf{w}$ adopts the minimum mean square error (MMSE) receiver. Defining $\mathbf{U} = \mathbf{u}\mathbf{u}^H$, $\mathbf{V} = \mathbf{v}\mathbf{v}^H$, $\mathbf{g}_{D,k,i}^{\text{cp}} = \mathbf{G}_{D,k}^* \mathbf{b}_{\text{cp},i}^*$, $\mathbf{g}_{D,k,i}^{\text{cc}} = \mathbf{G}_{D,k}^* \mathbf{b}_{\text{cc},i}^*$, $\mathbf{G}_{D,k,i}^{\text{cp}} = \mathbf{g}_{D,k,i}^{\text{cp}} (\mathbf{g}_{D,k,i}^{\text{cp}})^H$, and $\mathbf{G}_{D,k,i}^{\text{cc}} = \mathbf{g}_{D,k,i}^{\text{cc}} (\mathbf{g}_{D,k,i}^{\text{cc}})^H$, (11) is converted as

$$\min_{\substack{\{\mathbf{V}\succeq 0,\\ \mathbf{U}\succeq 0\}}} \{\mathbf{V}, \mathbf{U}\} \tag{14a}$$

$$\text{s.t.} \quad \frac{\text{Tr}(\mathbf{G}_{D,k,k}^{\text{cc}} \mathbf{U})}{r_{\min,k}} \geq \sum_{i=k+1}^{K} \text{Tr}(\mathbf{G}_{D,k,i}^{\text{cc}} \mathbf{U}) + \sum_{i=1}^{K} \text{Tr}(\mathbf{G}_{D,k,i}^{\text{cp}} \mathbf{U}) + \delta^2 \text{Tr}(\mathbf{U}), \forall k \in \mathcal{K}, \tag{14b}$$

$$\|\mathbf{b}_{\text{cp},k}^*\|^2 + \|\mathbf{b}_{\text{cc},k}^*\|^2 \leq \frac{T_{ET}\eta_k \text{Tr}(\mathbf{G}_{E,k}^* (\mathbf{G}_{E,k}^*)^H \mathbf{V})}{T_{IT}} + \frac{Q_{\text{ini},k}}{T_{IT}}, \forall k \in \mathcal{K}, \tag{14c}$$

$$\text{Tr}(\mathbf{V}) \leq P_{\max,A}, \tag{14d}$$

$$\text{Rank}(\mathbf{V}) = 1, \quad \text{Rank}(\mathbf{U}) = 1. \tag{14e}$$

(14) is non-convex because of the rank-one constraint (14e). According to matrix theory, we have

$$\text{Tr}(\mathbf{V}) - \lambda_{\max}(\mathbf{V}) \geq 0, \tag{15}$$

$$\text{Tr}(\mathbf{U}) - \lambda_{\max}(\mathbf{U}) \geq 0, \tag{16}$$

where $\lambda_{\max}(\mathbf{V})$ and $\lambda_{\max}(\mathbf{U})$ represent the maximum eigenvalue of $\mathbf{V}$ and $\mathbf{U}$, respectively. The equalities of (15)-(16) hold when the ranks of $\mathbf{V}$ and $\mathbf{U}$ are equivalent to 1. By replacing (14e) as (15)-(16) and integrating them into the objective function, problem (14) is transformed as

$$\min_{\{\mathbf{V}\succeq 0, \mathbf{U}\succeq 0\}} \text{Tr}(\mathbf{V}) - \lambda_{\max}(\mathbf{V}) + \text{Tr}(\mathbf{U}) - \lambda_{\max}(\mathbf{U}) \tag{17a}$$

$$\text{s.t.} \quad \text{(14b)-(14d)}. \tag{17b}$$

Problem (17) is still non-convex due to the non-concave eigenvalue function. Based on the successive convex approximation method, (17) can be convexified as

$$\min_{\substack{\{\mathbf{V}\succeq 0,\\ \mathbf{U}\succeq 0\}}} \ \mathrm{Tr}(\mathbf{V})-(\mathbf{v}_{\max}^{(i)})^H\mathbf{V}\mathbf{v}_{\max}^{(i)}+\mathrm{Tr}(\mathbf{U})-(\mathbf{u}_{\max}^{(i)})^H\mathbf{U}\mathbf{u}_{\max}^{(i)} \tag{18a}$$

$$\text{s.t.} \quad \text{(14b)-(14d)}, \tag{18b}$$

where $\mathbf{v}_{\max}^{(i)}$ and $\mathbf{u}_{\max}^{(i)}$ denote the eigenvectors associated with the maximum eigenvalue of $\mathbf{V}$ and $\mathbf{U}$, respectively. The rank-one solution is acquired by iteratively solving the convex problem (18). Then, $\mathbf{v}^{(i)}$ and $\mathbf{u}^{(i)}$ will be obtained by exploiting the eigenvalue decomposition, i.e., $\mathbf{v}^{(i)}=\sqrt{\lambda_{\max}(\mathbf{V}^{(i)})}\mathbf{v}_{\max}^{(i)}$ and $\mathbf{u}^{(i)}=\sqrt{\lambda_{\max}(\mathbf{U}^{(i)})}\mathbf{u}_{\max}^{(i)}$, where $\mathbf{v}_{\max}^{(i)}$ and $\mathbf{u}_{\max}^{(i)}$ represent the eigenvectors associated with the maximum eigenvalue of $\mathbf{V}^{(i)}$ and $\mathbf{U}^{(i)}$, respectively.

B. Phase Shift Optimization Subproblem

Given $\{\mathbf{b}_{\mathrm{cc},k}^*,\mathbf{b}_{\mathrm{cp},k}^*,\mathbf{u}^*,\mathbf{w}^*,\mathbf{v}^*\}$, (10) is simplified to the following phase shift optimization subproblem

$$\min_{\substack{\Theta_E,\\ \Theta_D}} \sum_{k=1}^{K}|(\mathbf{w}^*)^H\mathbf{G}_{D,k}\mathbf{b}_{\mathrm{cp},k}^*-1|^2+\sum_{k=1}^{K}|(\mathbf{w}^*)^H\mathbf{G}_{D,k}\mathbf{b}_{\mathrm{cc},k}^*|^2 \tag{19a}$$

$$\text{s.t.} \ \frac{|(\mathbf{u}^*)^H\mathbf{G}_{D,k}\mathbf{b}_{\mathrm{cc},k}^*|^2}{\sum_{i=k+1}^{K}|(\mathbf{u}^*)^H\mathbf{G}_{D,k}\mathbf{b}_{\mathrm{cc},i}^*|^2+\sum_{i=1}^{K}|(\mathbf{u}^*)^H\mathbf{G}_{D,k}\mathbf{b}_{\mathrm{cp},i}^*|^2+\delta^2\|\mathbf{u}^*\|^2}\geq r_{\min,k},\forall k\in\mathcal{K}, \tag{19b}$$

$$\|\mathbf{b}_{\mathrm{cp},k}^*\|^2+\|\mathbf{b}_{\mathrm{cc},k}^*\|^2\leq\frac{T_{ET}\eta_k\|\mathbf{G}_{E,k}^H\mathbf{v}^*\|^2}{T_{IT}}+\frac{Q_{\mathrm{ini},k}}{T_{IT}},\forall k\in\mathcal{K}, \tag{19c}$$

$$\text{C3-C4}. \tag{19d}$$

Next, we will adopt the variable substitution technique to transform (19) to a more tractable form. Denoting $c_k=(\mathbf{w}^*)^H\mathbf{G}_{d,k}\mathbf{b}_{\mathrm{cp},k}^*-1$, $\mathbf{d}_k=(\mathbf{w}^*)^H\mathbf{H}^H\mathrm{diag}(\mathbf{G}_{r,k}\mathbf{b}_{\mathrm{cp},k}^*)$, $\mathbf{v}_D=[e^{j\theta_{D,1}},\cdots,e^{j\theta_{D,M}}]^T$, and $\hat{\mathbf{v}}_D=[\mathbf{v}_D^T,1]^T$, we have

$$|(\mathbf{w}^*)^H(\mathbf{G}_{d,k}+\mathbf{H}^H\Theta_D\mathbf{G}_{r,k})\mathbf{b}_{\mathrm{cp},k}^*-1|^2=|\mathbf{d}_k\mathbf{v}_D+c_k|^2$$
$$=\mathbf{v}_D^H\mathbf{d}_k^H\mathbf{d}_k\mathbf{v}_D+\mathbf{v}_D^H\mathbf{d}_k^Hc_k+c_k^H\mathbf{d}_k\mathbf{v}_D+c_k^Hc_k=\hat{\mathbf{v}}_D^H\mathbf{Z1}_k\hat{\mathbf{v}}_D, \tag{20}$$

where $\mathbf{Z1}_k=[\mathbf{d}_k^H\mathbf{d}_k,\mathbf{d}_k^Hc_k;c_k^H\mathbf{d}_k,c_k^Hc_k]$. Similarly, the following equalities hold

$$|(\mathbf{w}^*)^H(\mathbf{G}_{d,k}+\mathbf{H}^H\Theta_D\mathbf{G}_{r,k})\mathbf{b}_{\mathrm{cc},k}^*|^2=\hat{\mathbf{v}}_D^H\mathbf{Z2}_k\hat{\mathbf{v}}_D, \tag{21}$$

$$|(\mathbf{u}^*)^H(\mathbf{G}_{d,k}+\mathbf{H}^H\Theta_D\mathbf{G}_{r,k})\mathbf{b}_{\mathrm{cp},i}^*|^2=\hat{\mathbf{v}}_D^H\mathbf{Z3}_{k,i}\hat{\mathbf{v}}_D, \tag{22}$$

$$|(\mathbf{u}^*)^H(\mathbf{G}_{d,k}+\mathbf{H}^H\Theta_D\mathbf{G}_{r,k})\mathbf{b}_{\mathrm{cc},i}^*|^2=\hat{\mathbf{v}}_D^H\mathbf{Z4}_{k,i}\hat{\mathbf{v}}_D, \tag{23}$$

where $e_k=(\mathbf{w}^*)^H\mathbf{G}_{d,k}\mathbf{b}_{\mathrm{cc},k}^*$, $\mathbf{f}_k=(\mathbf{w}^*)^H\mathbf{H}^H\mathrm{diag}(\mathbf{G}_{r,k}\mathbf{b}_{\mathrm{cc},k}^*)$, $m_{k,i}=(\mathbf{u}^*)^H\mathbf{G}_{d,k}\mathbf{b}_{\mathrm{cp},i}^*$, $\mathbf{q}_{k,i}=(\mathbf{u}^*)^H\mathbf{H}^H\mathrm{diag}(\mathbf{G}_{r,k}\mathbf{b}_{\mathrm{cp},i}^*)$, $h_{k,i}=(\mathbf{u}^*)^H\mathbf{G}_{d,k}\mathbf{b}_{\mathrm{cc},i}^*$, $\mathbf{l}_{k,i}=(\mathbf{u}^*)^H\mathbf{H}^H\mathrm{diag}(\mathbf{G}_{r,k}\mathbf{b}_{\mathrm{cc},i}^*)$,

$$\mathbf{Z2}_k=\begin{bmatrix}\mathbf{f}_k^H\mathbf{f}_k & \mathbf{f}_k^He_k\\ e_k^H\mathbf{f}_k & e_k^He_k\end{bmatrix},$$
$$\mathbf{Z3}_{k,i}=\begin{bmatrix}\mathbf{q}_{k,i}^H\mathbf{q}_{k,i} & \mathbf{q}_{k,i}^Hm_{k,i}\\ m_{k,i}^H\mathbf{q}_{k,i} & m_{k,i}^Hm_{k,i}\end{bmatrix}, \tag{24}$$
$$\mathbf{Z4}_{k,i}=\begin{bmatrix}\mathbf{l}_{k,i}^H\mathbf{l}_{k,i} & \mathbf{l}_{k,i}^Hh_{k,i}\\ h_{k,i}^H\mathbf{l}_{k,i} & h_{k,i}^Hh_{k,i}\end{bmatrix}.$$

Meanwhile, we have

$$\|(\mathbf{G}_{d,k}^H+\mathbf{G}_{r,k}^H\Theta_E\mathbf{H})\mathbf{v}^*\|^2=\hat{\mathbf{v}}_E^H\mathbf{Z5}_k\hat{\mathbf{v}}_E, \tag{25}$$

where $\mathbf{v}_E=[e^{j\theta_{E,1}},e^{j\theta_{E,2}},\cdots,e^{j\theta_{E,M}}]^T$, $\hat{\mathbf{v}}_E=[\mathbf{v}_E^T,1]^T$, $\mathbf{Z5}_k=[\mathrm{diag}((\mathbf{v}^*)^H\mathbf{H}^H)\mathbf{G}_{r,k}\mathbf{G}_{r,k}^H\mathrm{diag}(\mathbf{H}\mathbf{v}^*),$ $\mathrm{diag}((\mathbf{v}^*)^H\mathbf{H}^H)\mathbf{G}_{r,k}\mathbf{G}_{d,k}^H\mathbf{v}^*;(\mathbf{v}^*)^H\mathbf{G}_{d,k}\mathbf{G}_{r,k}^H\mathrm{diag}(\mathbf{H}\mathbf{v}^*),$ $(\mathbf{v}^*)^H\mathbf{G}_{d,k}\mathbf{G}_{d,k}^H\mathbf{v}^*]$.

According to (20)-(23) and (25), the phase shift optimization subproblem (19) is rewritten as

$$\min_{\substack{\hat{\mathbf{V}}_E\succeq 0,\\ \hat{\mathbf{V}}_D\succeq 0}} \ \sum_{k=1}^{K}\mathrm{Tr}(\mathbf{Z1}_k\hat{\mathbf{V}}_D)+\sum_{k=1}^{K}\mathrm{Tr}(\mathbf{Z2}_k\hat{\mathbf{V}}_D) \tag{26a}$$

$$\text{s.t.} \ \frac{\mathrm{Tr}(\mathbf{Z4}_{k,k}\hat{\mathbf{V}}_D)}{r_{\min,k}}\geq\sum_{i=k+1}^{K}\mathrm{Tr}(\mathbf{Z4}_{k,i}\hat{\mathbf{V}}_D)+\sum_{i=1}^{K}\mathrm{Tr}(\mathbf{Z3}_{k,i}\hat{\mathbf{V}}_D)+\delta^2\|\mathbf{u}^*\|^2,\forall k\in\mathcal{K}, \tag{26b}$$

$$\|\mathbf{b}_{\mathrm{cp},k}^*\|^2+\|\mathbf{b}_{\mathrm{cc},k}^*\|^2\leq\frac{T_{ET}\eta_k\mathrm{Tr}(\mathbf{Z5}_k\hat{\mathbf{V}}_E)}{T_{IT}}+\frac{Q_{\mathrm{ini},k}}{T_{IT}},\forall k\in\mathcal{K}, \tag{26c}$$

$$[\hat{\mathbf{V}}_E]_{mm}=1,\ [\hat{\mathbf{V}}_D]_{mm}=1,m\in\{\mathcal{M},M+1\}, \tag{26d}$$

$$\mathrm{Rank}(\hat{\mathbf{V}}_E)=1,\quad\mathrm{Rank}(\hat{\mathbf{V}}_D)=1, \tag{26e}$$

where $\hat{\mathbf{V}}_E=\hat{\mathbf{v}}_E^H\hat{\mathbf{v}}_E$ and $\hat{\mathbf{V}}_D=\hat{\mathbf{v}}_D\hat{\mathbf{v}}_D^H$. Similar to Section III-A, the penalty function-based algorithm is utilized to tackle the rank-one constraint (26e). Therefore, (26) is transformed to the following convex problem

$$\min_{\substack{\hat{\mathbf{V}}_E\succeq 0,\\ \hat{\mathbf{V}}_D\succeq 0}} \ \sum_{k=1}^{K}\mathrm{Tr}(\mathbf{Z1}_k\hat{\mathbf{V}}_D)+\sum_{k=1}^{K}\mathrm{Tr}(\mathbf{Z2}_k\hat{\mathbf{V}}_D)+\chi_1(\mathrm{Tr}(\hat{\mathbf{V}}_D)-(\mathbf{v}_{D,\max}^{(i)})^H\hat{\mathbf{V}}_D\mathbf{v}_{D,\max}^{(i)}+\mathrm{Tr}(\hat{\mathbf{V}}_E)-(\mathbf{v}_{E,\max}^{(i)})^H\hat{\mathbf{V}}_E\mathbf{v}_{E,\max}^{(i)}) \tag{27a}$$

$$\text{s.t.} \quad \text{(26b)-(26d)}, \tag{27b}$$

where χ_1 denotes the penalty factor, $\mathbf{v}_{D,\max}^{(i)}$ and $\mathbf{v}_{E,\max}^{(i)}$ stand for the eigenvectors associated with maximum eigenvalue of $\hat{\mathbf{V}}_E$ and $\hat{\mathbf{V}}_D$, respectively.

C. Transmit Beamforming Optimization Subproblem

For given $\{\Theta_E^*, \Theta_D^*, \mathbf{u}^*, \mathbf{w}^*, \mathbf{v}^*\}$, (10) is reduced as the transmit beamforming optimization subproblem

$$\min_{\substack{\{\mathbf{b}_{\text{cc},k},\\ \mathbf{b}_{\text{cp},k}\}}} \sum_{k=1}^{K} |(\mathbf{w}^*)^H \mathbf{G}_{D,k}^* \mathbf{b}_{\text{cp},k} - 1|^2 + \sum_{k=1}^{K} |(\mathbf{w}^*)^H \mathbf{G}_{D,k}^* \mathbf{b}_{\text{cc},k}|^2 \tag{28a}$$

$$\text{s.t.} \quad \frac{|(\mathbf{u}^*)^H \mathbf{G}_{D,k}^* \mathbf{b}_{\text{cc},k}|^2}{\sum_{i=k+1}^{K} |(\mathbf{u}^*)^H \mathbf{G}_{D,k}^* \mathbf{b}_{\text{cc},i}|^2 + \sum_{i=1}^{K} |(\mathbf{u}^*)^H \mathbf{G}_{D,k}^* \mathbf{b}_{\text{cp},i}|^2 + \delta^2 \|\mathbf{u}^*\|^2} \geq r_{\min,k}, \forall k \in \mathcal{K}, \tag{28b}$$

$$\|\mathbf{b}_{\text{cp},k}\|^2 + \|\mathbf{b}_{\text{cc},k}\|^2 \leq \frac{T_{ET}\eta_k \|(\mathbf{G}_{E,k}^*)^H \mathbf{v}^*\|^2}{T_{IT}} + \frac{Q_{\text{ini},k}}{T_{IT}}, \forall k \in \mathcal{K}. \tag{28c}$$

According to the principle of matrix operations, we have

$$|(\mathbf{w}^*)^H \mathbf{G}_{D,k}^* \mathbf{b}_{\text{cp},k} - 1|^2 = \mathbf{b}_{\text{cp},k}^H (\mathbf{G}_{D,k}^*)^H (\mathbf{w}^*)(\mathbf{w}^*)^H \mathbf{G}_{D,k}^* \mathbf{b}_{\text{cp},k} - \mathbf{b}_{\text{cp},k}^H (\mathbf{G}_{D,k}^*)^H \mathbf{w}^* - (\mathbf{w}^*)^H (\mathbf{G}_{D,k}^*) \mathbf{b}_{\text{cp},k} + 1 = \text{Tr}(\mathbf{J1}_k \hat{\mathbf{B}}_{\text{cp},k}), \tag{29}$$

$$|(\mathbf{u}^*)^H \mathbf{G}_{D,k}^* \mathbf{b}_{\text{cp},k}|^2 = \text{Tr}(\mathbf{J2}_k \hat{\mathbf{B}}_{\text{cp},k}), \tag{30}$$

where $\hat{\mathbf{b}}_{\text{cp},k} = [\mathbf{b}_{\text{cp},k}^T 1]^T$, $\hat{\mathbf{B}}_{\text{cp},k} = \hat{\mathbf{b}}_{\text{cp},k} \hat{\mathbf{b}}_{\text{cp},k}^H$,

$$\mathbf{J1}_k = \begin{bmatrix} (\mathbf{G}_{D,k}^*)^H (\mathbf{w}^*)(\mathbf{w}^*)^H (\mathbf{G}_{D,k}^*) & -(\mathbf{G}_{D,k}^*)^H \mathbf{w}^* \\ -(\mathbf{w}^*)^H \mathbf{G}_{D,k}^* & 1 \end{bmatrix},$$
$$\mathbf{J2}_k = \begin{bmatrix} (\mathbf{G}_{D,k}^*)^H (\mathbf{u}^*)(\mathbf{u}^*)^H \mathbf{G}_{D,k}^* & \mathbf{0}_{N_I \times 1} \\ \mathbf{0}_{1 \times N_I} & 0 \end{bmatrix}. \tag{31}$$

Defining $\mathbf{B}_{\text{cc},k} = \mathbf{b}_{\text{cc},k} \mathbf{b}_{\text{cc},k}^H$, and integrating (29)-(30) into (28), the transmit beamforming optimization subproblem is rewritten as

$$\min_{\substack{\{\mathbf{B}_{\text{cc},k} \succeq 0,\\ \hat{\mathbf{B}}_{\text{cp},k} \succeq 0\}}} \sum_{k=1}^{K} \text{Tr}((\mathbf{G}_{D,k}^*)^H \mathbf{w}^* (\mathbf{w}^*)^H \mathbf{G}_{D,k}^* \mathbf{B}_{\text{cc},k}) + \sum_{k=1}^{K} \text{Tr}(\mathbf{J1}_k \hat{\mathbf{B}}_{\text{cp},k}) \tag{32a}$$

$$\text{s.t.} \quad \frac{\text{Tr}((\mathbf{G}_{D,k}^*)^H \mathbf{u}^* (\mathbf{u}^*)^H \mathbf{G}_{D,k}^* \mathbf{B}_{\text{cc},k})}{r_{\min,k}} \geq \sum_{i=k+1}^{K} \text{Tr}((\mathbf{G}_{D,k}^*)^H \mathbf{u}^* (\mathbf{u}^*)^H \mathbf{G}_{D,k}^* \mathbf{B}_{\text{cc},i}) + \sum_{i=1}^{K} \text{Tr}(\mathbf{J2}_k \hat{\mathbf{B}}_{\text{cp},i}) + \delta^2 \|\mathbf{u}^*\|^2, \forall k \in \mathcal{K}, \tag{32b}$$

$$\text{Tr}(\hat{\mathbf{B}}_{\text{cp},k}) + \text{Tr}(\mathbf{B}_{\text{cc},k}) \leq 1 + \frac{T_{ET}\eta_k \|(\mathbf{G}_{E,k}^*)^H \mathbf{v}^*\|^2}{T_{IT}} + \frac{Q_{\text{ini},k}}{T_{IT}}, \forall k \in \mathcal{K}, \tag{32c}$$

$$[\hat{\mathbf{B}}_{\text{cp},k}]_{N_I+1, N_I+1} = 1, \forall k \in \mathcal{K}, \tag{32d}$$

$$\text{Rank}(\mathbf{B}_{\text{cc},k}) = 1, \quad \text{Rank}(\hat{\mathbf{B}}_{\text{cp},k}) = 1, \forall k \in \mathcal{K}. \tag{32e}$$

Similarly, the penalty function-based iterative algorithm is utilized to tackle the rank-one constraint (32e). Therefore, (32) is reformulated as the following convex problem

$$\min_{\substack{\{\mathbf{B}_{\text{cc},k} \succeq 0,\\ \hat{\mathbf{B}}_{\text{cp},k} \succeq 0\}}} \sum_{k=1}^{K} \text{Tr}(\mathbf{J1}_k \hat{\mathbf{B}}_{\text{cp},k}) + \sum_{k=1}^{K} \text{Tr}((\mathbf{G}_{D,k}^*)^H \mathbf{w}^* (\mathbf{w}^*)^H \mathbf{G}_{D,k}^* \mathbf{B}_{\text{cc},k}) + \chi_2 (\sum_{k=1}^{K} (\text{Tr}(\mathbf{B}_{\text{cc},k}) - (\mathbf{b}_{\max,\text{cc},k}^{(i)})^H \mathbf{B}_{\text{cc},k} \mathbf{b}_{\max,\text{cc},k}^{(i)}) + \sum_{k=1}^{K} (\text{Tr}(\hat{\mathbf{B}}_{\text{cp},k}) - (\mathbf{b}_{\max,\text{cp},k}^{(i)})^H \hat{\mathbf{B}}_{\text{cp},k} \mathbf{b}_{\max,\text{cp},k}^{(i)})) \tag{33a}$$

$$\text{s.t.} \quad \text{(32b)-(32d)}, \tag{33b}$$

where χ_2 represents the penalty factor, $\mathbf{b}_{\max,\text{cc},k}^{(i)}$ and $\mathbf{b}_{\max,\text{cp},k}^{(i)}$ denote the eigenvectors with the maximum eigenvalue of $\mathbf{B}_{\text{cc},k}$ and $\hat{\mathbf{B}}_{\text{cp},k}$, respectively.

D. Algorithm, Convergence and Complexity

As described in above subsections, this paper develops an alternating optimization framework to solve the MSE minimization problem (10) inspired by the block coordinate descent method. The optimization variables of original problem (10) are divided into three blocks. Then, the receive beamforming strategy $\{\mathbf{u}, \mathbf{w}, \mathbf{v}\}$, the phase shift optimization strategy $\{\Theta_E, \Theta_D\}$, and transmit beamforming strategy $\{\mathbf{b}_{\text{cc},k}, \mathbf{b}_{\text{cp},k}\}$ are alternately optimized by solving (11), (19) and (28), respectively, while keeping the other variables fixed. The details of the proposed method are elaborated in Algorithm 1. Then, we prove the convergence of Algorithm 1, and further analyze its computational complexity.

Convergence: Defining $\text{MSE}(\mathbf{w}^{(n)}, \mathbf{v}^{(n)}, \mathbf{u}^{(n)}, \Theta_E^{(n)}, \Theta_D^{(n)}, \mathbf{b}_{\text{cc},k}^{(n)}, \mathbf{b}_{\text{cp},k}^{(n)})$ as the objective function of (10) at the n-th iteration. Given $\{\Theta_E^{(n)}, \Theta_D^{(n)}, \mathbf{b}_{\text{cc},k}^{(n)}, \mathbf{b}_{\text{cp},k}^{(n)}\}$, the optimal receive beamforming is designed by solving (11), it follows that

$$\begin{aligned} &\text{MSE}(\mathbf{w}^{(n)}, \mathbf{v}^{(n)}, \mathbf{u}^{(n)}, \Theta_E^{(n)}, \Theta_D^{(n)}, \mathbf{b}_{\text{cc},k}^{(n)}, \mathbf{b}_{\text{cp},k}^{(n)}) \\ &\overset{(a1)}{\geq} \text{MSE}(\mathbf{w}^{(n+1)}, \mathbf{v}^{(n)}, \mathbf{u}^{(n)}, \Theta_E^{(n)}, \Theta_D^{(n)}, \mathbf{b}_{\text{cc},k}^{(n)}, \mathbf{b}_{\text{cp},k}^{(n)}) \\ &\overset{(a2)}{=} \text{MSE}(\mathbf{w}^{(n+1)}, \mathbf{v}^{(n+1)}, \mathbf{u}^{(n+1)}, \Theta_E^{(n)}, \Theta_D^{(n)}, \mathbf{b}_{\text{cc},k}^{(n)}, \mathbf{b}_{\text{cp},k}^{(n)}), \end{aligned} \tag{34}$$

where $(a1)$ holds because the optimal $\mathbf{w}^{(n+1)}$ is obtained to minimize the MSE according to *Theorem 1*, and $(a2)$ holds because the MSE is not related to $\{\mathbf{v}^{(n+1)}, \mathbf{u}^{(n+1)}\}$. Meanwhile, given $\{\mathbf{w}^{(n+1)}, \mathbf{v}^{(n+1)}, \mathbf{u}^{(n+1)}, \mathbf{b}_{\text{cc},k}^{(n)}, \mathbf{b}_{\text{cp},k}^{(n)}\}$, the optimal phase shift matrix $\{\Theta_E^{(n+1)}, \Theta_D^{(n+1)}\}$ is obtained by solving (19) for minimizing the MSE. Hence, we have

$$\begin{aligned} &\text{MSE}(\mathbf{w}^{(n+1)}, \mathbf{v}^{(n+1)}, \mathbf{u}^{(n+1)}, \Theta_E^{(n)}, \Theta_D^{(n)}, \mathbf{b}_{\text{cc},k}^{(n)}, \mathbf{b}_{\text{cp},k}^{(n)}) \geq \\ &\text{MSE}(\mathbf{w}^{(n+1)}, \mathbf{v}^{(n+1)}, \mathbf{u}^{(n+1)}, \Theta_E^{(n+1)}, \Theta_D^{(n+1)}, \mathbf{b}_{\text{cc},k}^{(n)}, \mathbf{b}_{\text{cp},k}^{(n)}). \end{aligned} \tag{35}$$

Given $\{\mathbf{w}^{(n+1)}, \mathbf{v}^{(n+1)}, \mathbf{u}^{(n+1)}, \Theta_E^{(n+1)}, \Theta_D^{(n+1)}\}$, the optimal transmit beamforming $\{\mathbf{b}_{\text{cc},k}^{(n+1)}, \mathbf{b}_{\text{cp},k}^{(n+1)}\}$ is achieved by solv-

Algorithm 1: Proposed method to solve the MSE minimization problem (10)

1 Set the iteration factor $n = 0$ and $i = 0$. Initialize a feasible solution $\{\mathbf{u}^{(0)}, \mathbf{v}^{(0)}, \Theta_E^{(0)}, \Theta_D^{(0)}, \mathbf{b}_{\text{cc},k}^{(0)}, \mathbf{b}_{\text{cp},k}^{(0)}\}$.
2 **Repeat:**
3 Update $n = n + 1$.
4 Calculate the optimal $\mathbf{w}^{(n)}$ according to (12).
5 **Repeat:**
6 Update $i = i + 1$.
7 Given $\{\mathbf{w}^{(n)}, \Theta_E^{(n-1)}, \Theta_D^{(n-1)}, \mathbf{b}_{\text{cc},k}^{(n-1)}, \mathbf{b}_{\text{cp},k}^{(n-1)}\}$, obtain $\{\mathbf{U}^{(i)}, \mathbf{V}^{(i)}\}$ by solving (18).
8 **Until** convergence.
9 Recovery $\mathbf{u}^{(n)} = \sqrt{\lambda_{\max}(\mathbf{U}^{(i)})}\mathbf{u}_{\max}^{(i)}$ and $\mathbf{v}^{(n)} = \sqrt{\lambda_{\max}(\mathbf{V}^{(i)})}\mathbf{v}_{\max}^{(i)}$, and set $i = 0$.
10 **Repeat:**
11 Update $i = i + 1$.
12 Given $\{\mathbf{u}^{(n)}, \mathbf{v}^{(n)}, \mathbf{w}^{(n)}, \mathbf{b}_{\text{cc},k}^{(n-1)}, \mathbf{b}_{\text{cp},k}^{(n-1)}\}$, acquire $\{\hat{\mathbf{V}}_E^{(i)}, \hat{\mathbf{V}}_D^{(i)}\}$ by solving (27).
13 **Until** convergence.
14 Recovery $\Theta_D^{(n)} = \text{diag}(\sqrt{\lambda_{\max}(\hat{\mathbf{V}}_D^{(i)})}\mathbf{v}_{D,\max}^{(i)}(1:M))$ and $\Theta_E^{(n)} = \text{diag}(\sqrt{\lambda_{\max}(\hat{\mathbf{V}}_E^{(i)})}\mathbf{v}_{E,\max}^{(i)}(1:M))$, and set $i = 0$.
15 **Repeat:**
16 Update $i = i + 1$.
17 Given $\{\mathbf{u}^{(n)}, \mathbf{v}^{(n)}, \mathbf{w}^{(n)}, \Theta_D^{(n)}, \Theta_E^{(n)}\}$, obtain $\{\mathbf{B}_{\text{cc},k}^{(i)}, \hat{\mathbf{B}}_{\text{cp},k}^{(i)}\}$ by solving (33).
18 **Until** convergence.
19 Recovery $\mathbf{b}_{\text{cc},k}^{(n)} = \sqrt{\lambda_{\max}(\mathbf{B}_{\text{cc},k}^{(i)})}\mathbf{b}_{\max,\text{cc},k}^{(i)}$ and $\mathbf{b}_{\text{cp},k}^{(n)} = \sqrt{\lambda_{\max}(\hat{\mathbf{B}}_{\text{cp},k}^{(i)})}\mathbf{b}_{\max,\text{cp},k}^{(i)}(1:N_I)$, and set $i = 0$.
20 **Until** convergence.
21 **Output:** optimal solution $\{\mathbf{u}, \mathbf{v}, \mathbf{w}, \Theta_E, \Theta_D, \mathbf{b}_{\text{cc},k}, \mathbf{b}_{\text{cp},k}\}$.

ing (28), and it yields that

$$\text{MSE}(\mathbf{w}^{(n+1)}, \mathbf{v}^{(n+1)}, \mathbf{u}^{(n+1)}, \Theta_E^{(n+1)}, \Theta_D^{(n+1)}, \mathbf{b}_{\text{cc},k}^{(n)}, \mathbf{b}_{\text{cp},k}^{(n)}) \geq \text{MSE}(\mathbf{w}^{(n+1)}, \mathbf{v}^{(n+1)}, \mathbf{u}^{(n+1)}, \Theta_E^{(n+1)}, \Theta_D^{(n+1)}, \mathbf{b}_{\text{cc},k}^{(n+1)}, \mathbf{b}_{\text{cp},k}^{(n+1)}). \tag{36}$$

According to above analysis, the objective function of (10) keeps non-increasing after each iteration. Combined with the boundedness of MSE, we derive that the proposed iterative method can converge to a suboptimal solution within a finite number of iterations.

Computational Complexity: The computational complexity of Algorithm 1 is expressed as the product of the iteration number and per-iteration complexity. In each iteration, three subproblems are solved sequentially, and the corresponding complexity is illustrated as follows.

- *Energy and Receive beamforming optimization subproblem:* In steps 4-9, Algorithm 1 is executed to acquire the optimal energy and receive beamforming strategy $\{\mathbf{w}^{(n)}, \mathbf{v}^{(n)}, \mathbf{u}^{(n)}\}$. The optimal $\mathbf{w}^{(n)}$ is derived in closed-form expression, and the corresponding complexity is negligible. To obtain optimal $\{\mathbf{v}^{(n)}, \mathbf{u}^{(n)}\}$, the interior point method-based solver is called to solve (18) in each iteration with $2K + 1$ constraints and $2N_A^2$ variables. Therefore, the computational complexity of receive beamforming optimization subproblem can be expressed as $\mathcal{O}(4T_1(2K + 1 + 2N_A^2)N_A^4\sqrt{2K+1}\log(\frac{1}{\epsilon_1}))$, where T_1 represents the iteration number in steps 5-8, and ϵ_1 denotes the convergence accuracy.
- *Phase shift optimization subproblem:* In steps 10-14, Algorithm 1 tends to acquire the optimal phase shift matrix $\{\Theta_D^{(n)}, \Theta_E^{(n)}\}$. Moreover, the penalty function-based algorithm is utilized to iteratively solve (27) consisting of $2(M+1)^2$ variables and $2(K+M+1)$ constraints, and the computational complexity is given by $\mathcal{O}(8T_2(M+1)^4((M+1)^2+K+M+1)\sqrt{2(K+M+1)}\log(\frac{1}{\epsilon_2}))$, where T_2 and ϵ_2 stand for the iteration number and convergence accuracy, respectively.
- *Transmit beamforming optimization subproblem:* In steps 15-19, Algorithm 1 concentrates on optimizing the transmit beamforming strategy $\{\mathbf{b}_{\text{cc},k}^{(n)}, \mathbf{b}_{\text{cp},k}^{(n)}\}$. The penalty function-based algorithm is applied to iteratively solve (33) with $N_I^2 + (N_I+1)^2$ variables and $3K$ constraints, and the complexity can be expressed as $\mathcal{O}(T_3(3K+N_I^2+(N_I+1)^2)(N_I^2+(N_I+1)^2)^2\sqrt{3K}\log(\frac{1}{\epsilon_3}))$, where T_3 and ϵ_3 indicate the iteration number and convergence accuracy, respectively.

Defining T_4 as the iteration number of Algorithm 1, the whole computational complexity of Algorithm 1 will be $\mathcal{O}(T_4(4T_1(2K+1+2N_A^2)N_A^4\sqrt{2K+1}\log(\frac{1}{\epsilon_1}) + 8T_2(M+1)^4((M+1)^2+K+M+1)\sqrt{2(K+M+1)}\log(\frac{1}{\epsilon_2}) + T_3(3K+N_I^2+(N_I+1)^2)(N_I^2+(N_I+1)^2)^2\sqrt{3K}\log(\frac{1}{\epsilon_3}))))$.

IV. Sum-rate maximization problem

This section investigates the sum rate maximization problem considering the maximum MSE constraint of the computation result, through jointly optimizing the transmit beamformer $\{\mathbf{b}_{\text{cc},k}, \mathbf{b}_{\text{cp},k}\}$ of IoT devices, phase shift matrix $\{\Theta_E, \Theta_D\}$ of IRS, energy beamformer $\mathbf{v}$ and receive beamformer $\{\mathbf{u}, \mathbf{w}\}$ of BS. The sum rate maximization problem is given by

$$\max_{\substack{\{\mathbf{v},\mathbf{u},\mathbf{w},\mathbf{b}_{\text{cc},k},\\ \mathbf{b}_{\text{cp},k},\Theta_E,\Theta_D\}}} \sum_{k=1}^{K} T_{IT}\log_2(1+\Gamma_k) \tag{37a}$$

$$\text{s.t.} \quad \text{MSE}(f, \hat{f}) \leq e_{\max}, \tag{37b}$$

$$\|\mathbf{b}_{\text{cp},k}\|^2 + \|\mathbf{b}_{\text{cc},k}\|^2 \leq \frac{T_{ET}\eta_k\|\mathbf{G}_{E,k}^H\mathbf{v}\|^2}{T_{IT}} + \frac{Q_{\text{ini},k}}{T_{IT}}, \forall k \in \mathcal{K}, \tag{37c}$$

$$0 \leq \theta_{E,m} \leq 2\pi, \quad 0 \leq \theta_{D,m} \leq 2\pi, \forall m \in \mathcal{M}, \tag{37d}$$

$$\|\mathbf{v}\|^2 \leq P_{\max,A}. \tag{37e}$$

As observed, (37) is non-convex problem due to the existence of co-channel interference signal and highly coupled optimization variables. To address it, this paper first utilizes

the *Lemma 1* to rewrite the non-convex and non-concave rate expression, and then develops an alternating optimization framework to decouple the coupled optimization variables.

Lemma 1: Denoting $f(b) = -ba + \ln(b) + 1$, it yields that

$$-\ln a = \max_{b>0} f(b). \tag{38}$$

The equality holds when $b = 1/a$. Defining $\mathbf{G}_{D,k} = \mathbf{G}_{d,k} + \mathbf{H}^H \Theta_D \mathbf{G}_{r,k}$, $a = \sum_{i=k+1}^{K} |\mathbf{u}^H \mathbf{G}_{D,k} \mathbf{b}_{\text{cc},i}|^2 + \sum_{i=1}^{K} |\mathbf{u}^H \mathbf{G}_{D,k} \mathbf{b}_{\text{cp},i}|^2 + \delta^2 \|\mathbf{u}\|^2$ and $b = y_k^{(n)}$, $\log_2(1+\Gamma_k)$ is rewritten as

$$\begin{aligned}
&\log_2(1+\Gamma_k) = \\
&\log_2\Big(\sum_{i=k}^{K} |\mathbf{u}^H \mathbf{G}_{D,k} \mathbf{b}_{\text{cc},i}|^2 + \sum_{i=1}^{K} |\mathbf{u}^H \mathbf{G}_{D,k} \mathbf{b}_{\text{cp},i}|^2 + \delta^2 \|\mathbf{u}\|^2\Big) \\
&- \log_2\Big(\sum_{i=k+1}^{K} |\mathbf{u}^H \mathbf{G}_{D,k} \mathbf{b}_{\text{cc},i}|^2 + \sum_{i=1}^{K} |\mathbf{u}^H \mathbf{G}_{D,k} \mathbf{b}_{\text{cp},i}|^2 + \delta^2 \|\mathbf{u}\|^2\Big) \\
&= \log_2\Big(\sum_{i=k}^{K} |\mathbf{u}^H \mathbf{G}_{D,k} \mathbf{b}_{\text{cc},i}|^2 + \sum_{i=1}^{K} |\mathbf{u}^H \mathbf{G}_{D,k} \mathbf{b}_{\text{cp},i}|^2 + \delta^2 \|\mathbf{u}\|^2\Big) + \\
&\frac{1}{\ln 2}\Big(-y_k^{(n)}\Big(\sum_{i=k+1}^{K} |\mathbf{u}^H \mathbf{G}_{D,k} \mathbf{b}_{\text{cc},i}|^2 + \sum_{i=1}^{K} |\mathbf{u}^H \mathbf{G}_{D,k} \mathbf{b}_{\text{cp},i}|^2 + \delta^2 \|\mathbf{u}\|^2\Big) \\
&+ \ln y_k^{(n)} + 1\Big).
\end{aligned} \tag{39}$$

Hence, the optimal solution of (37) is able to be acquired by iteratively solving the following problem

$$\begin{aligned}
\max_{\substack{\{\mathbf{v},\mathbf{u},\mathbf{w},\mathbf{b}_{\text{cc},k},\\ \mathbf{b}_{\text{cp},k},\Theta_E,\Theta_D\}}} \quad & \sum_{k=1}^{K} \log_2\Big(\sum_{i=k}^{K} |\mathbf{u}^H \mathbf{G}_{D,k} \mathbf{b}_{\text{cc},i}|^2 + \sum_{i=1}^{K} |\mathbf{u}^H \mathbf{G}_{D,k} \mathbf{b}_{\text{cp},i}|^2 \\
& + \delta^2 \|\mathbf{u}\|^2\Big) + \frac{1}{\ln 2}\Big(-y_k^{(n)}\Big(\sum_{i=k+1}^{K} |\mathbf{u}^H \mathbf{G}_{D,k} \mathbf{b}_{\text{cc},i}|^2 \\
& + \sum_{i=1}^{K} |\mathbf{u}^H \mathbf{G}_{D,k} \mathbf{b}_{\text{cp},i}|^2 + \delta^2 \|\mathbf{u}\|^2\Big) + \ln y_k^{(n)} + 1\Big)
\end{aligned} \tag{40a}$$

$$\begin{aligned}
\text{s.t.} \quad & \|\mathbf{b}_{\text{cp},k}\|^2 + \|\mathbf{b}_{\text{cc},k}\|^2 \le \frac{T_{ET}\eta_k \|\mathbf{G}_{E,k}^H \mathbf{v}\|^2}{T_{IT}} \\
& + \frac{Q_{\text{ini},k}}{T_{IT}}, \forall k \in \mathcal{K},
\end{aligned} \tag{40b}$$

$$\text{(37b), (37d)-(37e).} \tag{40c}$$

Based on the block coordinate descent method, (40) can be solved by iteratively solving three subproblems, namely receive beamforming optimization subproblem, phase shift optimization subproblem, and transmit beamforming optimization subproblem, which are elaborated in the following subsections.

A. Energy and Receive Beamforming Optimization Subproblem

Given $\{\mathbf{b}_{\text{cc},k}^*, \mathbf{b}_{\text{cp},k}^*, \Theta_E^*, \Theta_D^*\}$, (40) is reduced as

$$\begin{aligned}
\max_{\mathbf{v},\mathbf{u},\mathbf{w}} \quad & \sum_{k=1}^{K} \log_2\Big(\sum_{i=k}^{K} |\mathbf{u}^H \mathbf{G}_{D,k}^* \mathbf{b}_{\text{cc},i}^*|^2 + \sum_{i=1}^{K} |\mathbf{u}^H \mathbf{G}_{D,k}^* \mathbf{b}_{\text{cp},i}^*|^2 \\
& + \delta^2 \|\mathbf{u}\|^2\Big) + \frac{1}{\ln 2}\Big(-y_k^{(n)}\Big(\sum_{i=k+1}^{K} |\mathbf{u}^H \mathbf{G}_{D,k}^* \mathbf{b}_{\text{cc},i}^*|^2 + \\
& \sum_{i=1}^{K} |\mathbf{u}^H \mathbf{G}_{D,k}^* \mathbf{b}_{\text{cp},i}^*|^2 + \delta^2 \|\mathbf{u}\|^2\Big) + \ln y_k^{(n)} + 1\Big)
\end{aligned} \tag{41a}$$

$$\begin{aligned}
\text{s.t.} \quad & \sum_{k=1}^{K} |\mathbf{w}^H \mathbf{G}_{D,k}^* \mathbf{b}_{\text{cp},k}^* - 1|^2 + \sum_{k=1}^{K} |\mathbf{w}^H \mathbf{G}_{D,k}^* \mathbf{b}_{\text{cc},k}^*|^2 \\
& + \delta^2 \|\mathbf{w}\|^2 \le e_{\max},
\end{aligned} \tag{41b}$$

$$\begin{aligned}
& \|\mathbf{b}_{\text{cp},k}^*\|^2 + \|\mathbf{b}_{\text{cc},k}^*\|^2 \le \frac{T_{ET}\eta_k \|(\mathbf{G}_{E,k}^*)^H \mathbf{v}\|^2}{T_{IT}} \\
& + \frac{Q_{\text{ini},k}}{T_{IT}}, \forall k \in \mathcal{K},
\end{aligned} \tag{41c}$$

$$\|\mathbf{v}\|^2 \le P_{\max,A}. \tag{41d}$$

Similar to Section III-A, the optimal $\mathbf{w}$ adopts the MMSE beamforming method as given in (12). Defining $\mathbf{U} = \mathbf{u}\mathbf{u}^H$ and $\mathbf{V} = \mathbf{v}\mathbf{v}^H$, (41) is further transformed as

$$\begin{aligned}
\max_{\substack{\{\mathbf{V}\succeq 0,\\ \mathbf{U}\succeq 0\}}} \quad & \sum_{k=1}^{K} \log_2\Big(\sum_{i=k}^{K} \text{Tr}(\mathbf{G}_{D,k}^* \mathbf{b}_{\text{cc},i}^* (\mathbf{b}_{\text{cc},i}^*)^H (\mathbf{G}_{D,k}^*)^H \mathbf{U}) + \\
& \sum_{i=1}^{K} \text{Tr}(\mathbf{G}_{D,k}^* \mathbf{b}_{\text{cp},i}^* (\mathbf{b}_{\text{cp},i}^*)^H (\mathbf{G}_{D,k}^*)^H \mathbf{U}) + \delta^2 \text{Tr}(\mathbf{U})\Big) \\
& + \frac{1}{\ln 2}\Big(-y_k^{(n)}\Big(\sum_{i=k+1}^{K} \text{Tr}(\mathbf{G}_{D,k}^* \mathbf{b}_{\text{cc},i}^* (\mathbf{b}_{\text{cc},i}^*)^H (\mathbf{G}_{D,k}^*)^H \mathbf{U}) \\
& + \sum_{i=1}^{K} \text{Tr}(\mathbf{G}_{D,k}^* \mathbf{b}_{\text{cp},i}^* (\mathbf{b}_{\text{cp},i}^*)^H (\mathbf{G}_{D,k}^*)^H \mathbf{U}) + \delta^2 \text{Tr}(\mathbf{U})\Big) \\
& + \ln y_k^{(n)} + 1\Big)
\end{aligned} \tag{42a}$$

$$\begin{aligned}
\text{s.t.} \quad & \|\mathbf{b}_{\text{cp},k}^*\|^2 + \|\mathbf{b}_{\text{cc},k}^*\|^2 \le \frac{T_{ET}\eta_k \text{Tr}(\mathbf{G}_{E,k}^* (\mathbf{G}_{E,k}^*)^H \mathbf{V})}{T_{IT}} \\
& + \frac{Q_{\text{ini},k}}{T_{IT}}, \forall k \in \mathcal{K},
\end{aligned} \tag{42b}$$

$$\text{Tr}(\mathbf{V}) \le P_{\max,A}, \tag{42c}$$

$$\text{Rank}(\mathbf{U}) = 1, \quad \text{Rank}(\mathbf{V}) = 1. \tag{42d}$$

Furthermore, similar to the proposed penalty function-based method in Section III, the rank-one constraint (42d) can be removed by adding a penalty item at the objective function

(42a). Hence, (42) can be converted as

$$\begin{aligned}
&\sum_{k=1}^{K}\log_2(\sum_{i=k}^{K}\mathrm{Tr}(\mathbf{G}_{D,k}^{*}\mathbf{b}_{\mathrm{cc},i}^{*}(\mathbf{b}_{\mathrm{cc},i}^{*})^H(\mathbf{G}_{D,k}^{*})^H\mathbf{U})+\\
&\sum_{i=1}^{K}\mathrm{Tr}(\mathbf{G}_{D,k}^{*}\mathbf{b}_{\mathrm{cp},i}^{*}(\mathbf{b}_{\mathrm{cp},i}^{*})^H(\mathbf{G}_{D,k}^{*})^H\mathbf{U})+\delta^2\mathrm{Tr}(\mathbf{U}))+\\
\max_{\substack{\{\mathbf{V}\succeq 0,\\ \mathbf{U}\succeq 0\}}}\ &\frac{1}{\ln 2}(-y_k^{(n)}(\sum_{i=k+1}^{K}\mathrm{Tr}(\mathbf{G}_{D,k}^{*}\mathbf{b}_{\mathrm{cc},i}^{*}(\mathbf{b}_{\mathrm{cc},i}^{*})^H(\mathbf{G}_{D,k}^{*})^H\mathbf{U})\\
&+\sum_{i=1}^{K}\mathrm{Tr}(\mathbf{G}_{D,k}^{*}\mathbf{b}_{\mathrm{cp},i}^{*}(\mathbf{b}_{\mathrm{cp},i}^{*})^H(\mathbf{G}_{D,k}^{*})^H\mathbf{U})+\delta^2\mathrm{Tr}(\mathbf{U}))\\
&+\ln y_k^{(n)}+1)-\chi_3(\mathrm{Tr}(\mathbf{V})-(\mathbf{v}_{\max}^{(i)})^H\mathbf{V}\mathbf{v}_{\max}^{(i)}+\\
&\mathrm{Tr}(\mathbf{U})-(\mathbf{u}_{\max}^{(i)})^H\mathbf{U}\mathbf{u}_{\max}^{(i)})
\end{aligned}\tag{43a}$$

$$\text{s.t.}\qquad \text{(42b)-(42c)},\tag{43b}$$

where χ_3 is the penalty factor. Besides, the convex problem (43) can be solved by the convex toolbox, such as CVX or Yalmip [41].

B. Phase Shift Optimization Subproblem

Given $\{\mathbf{b}_{\mathrm{cc},k}^{*},\mathbf{b}_{\mathrm{cp},k}^{*},\mathbf{v}^{*},\mathbf{u}^{*},\mathbf{w}^{*}\}$, (40) is simplified as

$$\begin{aligned}
&\sum_{k=1}^{K}\log_2(\sum_{i=k}^{K}|(\mathbf{u}^{*})^H(\mathbf{G}_{d,k}+\mathbf{H}^H\Theta_D\mathbf{G}_{r,k})\mathbf{b}_{\mathrm{cc},i}^{*}|^2+\\
&\sum_{i=1}^{K}|(\mathbf{u}^{*})^H(\mathbf{G}_{d,k}+\mathbf{H}^H\Theta_D\mathbf{G}_{r,k})\mathbf{b}_{\mathrm{cp},i}^{*}|^2+\delta^2\|\mathbf{u}^{*}\|^2)+\\
\max_{\Theta_E,\Theta_D}\ &\frac{1}{\ln 2}(-y_k^{(n)}(\sum_{i=k+1}^{K}|(\mathbf{u}^{*})^H(\mathbf{G}_{d,k}+\mathbf{H}^H\Theta_D\mathbf{G}_{r,k})\mathbf{b}_{\mathrm{cc},i}^{*}|^2\\
&+\sum_{i=1}^{K}|(\mathbf{u}^{*})^H(\mathbf{G}_{d,k}+\mathbf{H}^H\Theta_D\mathbf{G}_{r,k})\mathbf{b}_{\mathrm{cp},i}^{*}|^2+\delta^2\|\mathbf{u}^{*}\|^2)\\
&+\ln y_k^{(n)}+1)
\end{aligned}\tag{44a}$$

$$\begin{aligned}
\text{s.t.}\ &\sum_{k=1}^{K}|(\mathbf{w}^{*})^H(\mathbf{G}_{d,k}+\mathbf{H}^H\Theta_D\mathbf{G}_{r,k})\mathbf{b}_{\mathrm{cp},k}^{*}-1|^2+\\
&\sum_{k=1}^{K}|(\mathbf{w}^{*})^H(\mathbf{G}_{d,k}+\mathbf{H}^H\Theta_D\mathbf{G}_{r,k})\mathbf{b}_{\mathrm{cc},k}^{*}|^2+\delta^2\|\mathbf{w}^{*}\|^2\\
&\le e_{\max},
\end{aligned}\tag{44b}$$

$$\begin{aligned}
&\|\mathbf{b}_{\mathrm{cp},k}^{*}\|^2+\|\mathbf{b}_{\mathrm{cc},k}^{*}\|^2\le\frac{T_{ET}\eta_k\|(\mathbf{G}_{d,k}^H+\mathbf{G}_{r,k}^H\Theta_E\mathbf{H})\mathbf{v}^{*}\|^2}{T_{IT}}\\
&+\frac{Q_{\mathrm{ini},k}}{T_{IT}},\forall k\in\mathcal{K},
\end{aligned}\tag{44c}$$

$$0\le\theta_{E,m}\le 2\pi,\quad 0\le\theta_{D,m}\le 2\pi,\forall m\in\mathcal{M}.\tag{44d}$$

According to the similar transformation in Section III-B, (44) is transformed as

$$\begin{aligned}
&\sum_{k=1}^{K}\log_2(\sum_{i=k}^{K}\mathrm{Tr}(\mathbf{Z4}_{k,i}\hat{\mathbf{V}}_D)+\sum_{i=1}^{K}\mathrm{Tr}(\mathbf{Z3}_{k,i}\hat{\mathbf{V}}_D)+\delta^2\|\mathbf{u}^{*}\|^2)\\
\max_{\substack{\hat{\mathbf{V}}_D\succeq 0,\\ \hat{\mathbf{V}}_E\succeq 0}}\ &+\frac{1}{\ln 2}(-y_k^{(n)}(\sum_{i=k+1}^{K}\mathrm{Tr}(\mathbf{Z4}_{k,i}\hat{\mathbf{V}}_D)+\sum_{i=1}^{K}\mathrm{Tr}(\mathbf{Z3}_{k,i}\hat{\mathbf{V}}_D)\\
&+\delta^2\|\mathbf{u}^{*}\|^2)+\ln y_k^{(n)}+1)-\chi_4(\mathrm{Tr}(\hat{\mathbf{V}}_D)+\mathrm{Tr}(\hat{\mathbf{V}}_E)\\
&-(\mathbf{v}_{D,\max}^{(i)})^H\hat{\mathbf{V}}_D\mathbf{v}_{D,\max}^{(i)}-(\mathbf{v}_{E,\max}^{(i)})^H\hat{\mathbf{V}}_E\mathbf{v}_{E,\max}^{(i)})
\end{aligned}\tag{45a}$$

$$\begin{aligned}
\text{s.t.}\ &\sum_{k=1}^{K}\mathrm{Tr}(\mathbf{Z1}_k\hat{\mathbf{V}}_D)+\sum_{k=1}^{K}\mathrm{Tr}(\mathbf{Z2}_k\hat{\mathbf{V}}_D)+\delta^2\|\mathbf{w}^{*}\|^2\\
&\le e_{\max},
\end{aligned}\tag{45b}$$

$$\begin{aligned}
&\|\mathbf{b}_{\mathrm{cp},k}^{*}\|^2+\|\mathbf{b}_{\mathrm{cc},k}^{*}\|^2\le\frac{T_{ET}\eta_k\mathrm{Tr}(\mathbf{Z5}_k\hat{\mathbf{V}}_E)}{T_{IT}}\\
&+\frac{Q_{\mathrm{ini},k}}{T_{IT}},\forall k\in\mathcal{K},
\end{aligned}\tag{45c}$$

$$[\hat{\mathbf{V}}_E]_{mm}=1,\ [\hat{\mathbf{V}}_D]_{mm}=1,m\in\{\mathcal{M},M+1\},\tag{45d}$$

where χ_4 denotes the penalty factor. Meanwhile, the convex problem (45) can be solved by calling the classic convex methods integrated in CVX.

C. Transmit Beamforming Optimization Subproblem

Given $\{\mathbf{u}^{*},\mathbf{w}^{*},\mathbf{v}^{*},\Theta_E^{*},\Theta_D^{*}\}$, (40) is simplified as

$$\begin{aligned}
&\sum_{k=1}^{K}\log_2(\sum_{i=k}^{K}|\mathbf{u}^H\mathbf{G}_{D,k}^{*}\mathbf{b}_{\mathrm{cc},i}|^2+\sum_{i=1}^{K}|\mathbf{u}^H\mathbf{G}_{D,k}^{*}\mathbf{b}_{\mathrm{cp},i}|^2\\
\max_{\{\mathbf{b}_{\mathrm{cc},k},\mathbf{b}_{\mathrm{cp},k}\}}\ &+\delta^2\|\mathbf{u}^{*}\|^2)+\frac{1}{\ln 2}(-y_k^{(n)}(\sum_{i=k+1}^{K}|\mathbf{u}^H\mathbf{G}_{D,k}^{*}\mathbf{b}_{\mathrm{cc},i}|^2+\\
&\sum_{i=1}^{K}|\mathbf{u}^H\mathbf{G}_{D,k}^{*}\mathbf{b}_{\mathrm{cp},i}|^2+\delta^2\|\mathbf{u}^{*}\|^2)+\ln y_k^{(n)}+1)
\end{aligned}\tag{46a}$$

$$\begin{aligned}
\text{s.t.}\ &\sum_{k=1}^{K}|(\mathbf{w}^{*})^H\mathbf{G}_{D,k}^{*}\mathbf{b}_{\mathrm{cp},k}-1|^2+\sum_{k=1}^{K}|(\mathbf{w}^{*})^H\mathbf{G}_{D,k}^{*}\mathbf{b}_{\mathrm{cc},k}|^2\\
&+\delta^2\|\mathbf{w}^{*}\|^2\le e_{\max},
\end{aligned}\tag{46b}$$

$$\begin{aligned}
&\|\mathbf{b}_{\mathrm{cp},k}\|^2+\|\mathbf{b}_{\mathrm{cc},k}\|^2\le\frac{T_{ET}\eta_k\|(\mathbf{G}_{E,k}^{*})^H\mathbf{v}^{*}\|^2}{T_{IT}}\\
&+\frac{Q_{\mathrm{ini},k}}{T_{IT}},\forall k\in\mathcal{K}.
\end{aligned}\tag{46c}$$

By utilizing the similar transformation in Section III-C, (46) is converted as

$$\max_{\substack{\{\mathbf{B}_{\text{cc},k}\succeq 0,\\ \hat{\mathbf{B}}_{\text{cp},k}\succeq 0\}}} \sum_{k=1}^{K}\log_2(\sum_{i=k}^{K}\text{Tr}((\mathbf{G}_{D,k}^*)^H\mathbf{u}^*(\mathbf{u}^*)^H\mathbf{G}_{D,k}^*\mathbf{B}_{\text{cc},i})+ \sum_{i=1}^{K}\text{Tr}(\mathbf{J2}_k\hat{\mathbf{B}}_{\text{cp},i})+\delta^2\|\mathbf{u}^*\|^2)+ \frac{1}{\ln 2}(-y_k^{(n)}(\sum_{i=k+1}^{K}\text{Tr}((\mathbf{G}_{D,k}^*)^H\mathbf{u}^*(\mathbf{u}^*)^H\mathbf{G}_{D,k}^*\mathbf{B}_{\text{cc},i})+ \sum_{i=1}^{K}\text{Tr}(\mathbf{J2}_k\hat{\mathbf{B}}_{\text{cp},i})+\delta^2\|\mathbf{u}^*\|^2)+\ln y_k^{(n)}+1) - \chi_5(\sum_{k=1}^{K}(\text{Tr}(\mathbf{B}_{\text{cc},k})-(\mathbf{b}_{\text{max,cc},k}^{(i)})^H\mathbf{B}_{\text{cc},k}\mathbf{b}_{\text{max,cc},k}^{(i)}) + \sum_{k=1}^{K}(\text{Tr}(\hat{\mathbf{B}}_{\text{cp},k})-(\mathbf{b}_{\text{max,cp},k}^{(i)})^H\hat{\mathbf{B}}_{\text{cp},k}\mathbf{b}_{\text{max,cp},k}^{(i)})) \tag{47a}$$

$$\text{s.t.} \quad \sum_{k=1}^{K}\text{Tr}((\mathbf{G}_{D,k}^*)^H\mathbf{w}^*(\mathbf{w}^*)^H\mathbf{G}_{D,k}^*\mathbf{B}_{\text{cc},k}) \sum_{k=1}^{K}\text{Tr}(\mathbf{J1}_k\hat{\mathbf{B}}_{\text{cp},k})+\delta^2\|\mathbf{w}^*\|^2\le e_{\max}, \tag{47b}$$

$$\text{Tr}(\hat{\mathbf{B}}_{\text{cp},k})+\text{Tr}(\mathbf{B}_{\text{cc},k})\le 1+\frac{Q_{\text{ini},k}}{T_{IT}} + \frac{T_{ET}\eta_k\|(\mathbf{G}_{E,k}^*)^H\mathbf{v}^*\|^2}{T_{IT}},\forall k\in\mathcal{K}, \tag{47c}$$

$$[\hat{\mathbf{B}}_{\text{cp},k}]_{N_I+1,N_I+1}=1,\forall k\in\mathcal{K}, \tag{47d}$$

where χ_5 denotes the penalty factor. Due to the concave objective function and the linear constraints, (47) is a convex problem, which can be solved by various methods, such as interior-point method.

D. Algorithm, Convergence and Complexity

This subsection summarizes the whole procedure for solving the sum rate maximization problem (37) in Algorithm 2. Similar to Algorithm 1, the convergence of Algorithm 2 can be proved by the monotone bounded theorem. The achievable sum rate of (37) is non-decreasing through each iteration, since the three subproblems maximize the sum rate in an alternating manner. In addition, the sum rate is upper bounded due to the limited energy supply of IoT devices. Therefore, Algorithm 2 can converge to the optimal solution after several iterations.

The computational complexity of Algorithm 2 is comprised by the iteration number and per-iteration complexity. The whole complexity is written as $\mathcal{O}(T_8(4T_5(K+1+2N_A^2)N_A^4\sqrt{K+1}\log(\frac{1}{\epsilon_4})+4T_6(K+1+2(M+1)(M+2))(M+1)^4\sqrt{K+1+2(M+1)}\log(\frac{1}{\epsilon_5})+T_7(2K+1+N_I^2+(N_I+1)^2)(N_I^2+(N_I+1)^2)^2\sqrt{2K+1}\log(\frac{1}{\epsilon_6})))$, where T_8 denotes the iteration number of Algorithm 2, T_5, T_6 and T_7 represent the iteration number of the receive beamforming subproblem, phase shift optimization subproblem, and transmit beamforming optimization subproblem, respectively, ϵ_4, ϵ_5 and ϵ_6 stand for the corresponding convergence accuracy.

According to above descriptions, Algorithms 1-2 are developed to solve the non-convex MSE minimization problem and sum rate maximization problem with polynomial complexity order. In contrast, defining G_t as the candidate value size for each optimization variable, the complexity of exhaustive search algorithm is $\mathcal{O}(G_t^{3N_A+2KN_I+2M})$, which exponentially increases as N_A, K, N_I and M. In addition, the particle swarm optimization algorithm can be modified to solve the beamforming optimization problems with the complexity of $\mathcal{O}(I_tI_sI_f)$ [42], [43], where I_t denotes the iteration number,

Algorithm 2: Proposed method to solve the sum rate maximization problem (37)

1. Set the iteration factor $n=0$ and $i=0$. Initialize a feasible solution $\{\mathbf{u}^{(0)},\mathbf{v}^{(0)},\Theta_E^{(0)},\Theta_D^{(0)},\mathbf{b}_{\text{cc},k}^{(0)},\mathbf{b}_{\text{cp},k}^{(0)}\}$ and $y_k^{(0)}$.
2. **Repeat:**
3. Update $n=n+1$.
4. Calculate the optimal $\mathbf{w}^{(n)}$ according to (12).
5. **Repeat:**
6. Update $i=i+1$.
7. Given $\{\mathbf{w}^{(n)},y_k^{(n-1)},\Theta_E^{(n-1)},\Theta_D^{(n-1)},\mathbf{b}_{\text{cc},k}^{(n-1)},\mathbf{b}_{\text{cp},k}^{(n-1)}\}$, obtain $\{\mathbf{U}^{(i)},\mathbf{V}^{(i)}\}$ by solving (43).
8. **Until** convergence.
9. Recovery $\mathbf{u}^{(n)}=\sqrt{\lambda_{\max}(\mathbf{U}^{(i)})}\mathbf{u}_{\max}^{(i)}$ and $\mathbf{v}^{(n)}=\sqrt{\lambda_{\max}(\mathbf{V}^{(i)})}\mathbf{v}_{\max}^{(i)}$, and set $i=0$.
10. **Repeat:**
11. Update $i=i+1$.
12. Given $\{\mathbf{u}^{(n)},\mathbf{v}^{(n)},\mathbf{w}^{(n)},y_k^{(n-1)},\mathbf{b}_{\text{cc},k}^{(n-1)},\mathbf{b}_{\text{cp},k}^{(n-1)}\}$, acquire $\{\hat{\mathbf{V}}_E^{(i)},\hat{\mathbf{V}}_D^{(i)}\}$ by solving (45).
13. **Until** convergence.
14. Recovery $\Theta_D^{(n)}=\text{diag}(\sqrt{\lambda_{\max}(\hat{\mathbf{V}}_D^{(i)})}\mathbf{v}_{D,\max}^{(i)}(1:M))$ and $\Theta_E^{(n)}=\text{diag}(\sqrt{\lambda_{\max}(\hat{\mathbf{V}}_E^{(i)})}\mathbf{v}_{E,\max}^{(i)}(1:M))$, and set $i=0$.
15. **Repeat:**
16. Update $i=i+1$.
17. Given $\{\mathbf{u}^{(n)},\mathbf{v}^{(n)},\mathbf{w}^{(n)},\Theta_D^{(n)},\Theta_E^{(n)},y_k^{(n-1)}\}$, obtain $\{\mathbf{B}_{\text{cc},k}^{(i)},\hat{\mathbf{B}}_{\text{cp},k}^{(i)}\}$ by solving (47).
18. **Until** convergence.
19. Recovery $\mathbf{b}_{\text{cc},k}^{(n)}=\sqrt{\lambda_{\max}(\mathbf{B}_{\text{cc},k}^{(i)})}\mathbf{b}_{\text{max,cc},k}^{(i)}$ and $\mathbf{b}_{\text{cp},k}^{(n)}=\sqrt{\lambda_{\max}(\hat{\mathbf{B}}_{\text{cp},k}^{(i)})}\mathbf{b}_{\text{max,cp},k}^{(i)}(1:N_I)$, and set $i=0$.
20. Update $y_k^{(n)}=\frac{1}{\sum_{i=k+1}^{K}|(\mathbf{u}^{(n)})^H\mathbf{G}_{D,k}^{(n)}\mathbf{b}_{\text{cc},i}^{(n)}|^2+\sum_{i=1}^{K}|(\mathbf{u}^{(n)})^H\mathbf{G}_{D,k}^{(n)}\mathbf{b}_{\text{cp},i}^{(n)}|^2+\delta^2\|\mathbf{u}^{(n)}\|^2}$, where $\mathbf{G}_{D,k}^{(n)}=\mathbf{G}_{d,k}+\mathbf{H}^H\Theta_D^{(n)}\mathbf{G}_{r,k}$.
21. **Until** convergence.
22. **Output:** optimal solution $\{\mathbf{u},\mathbf{v},\mathbf{w},\Theta_E,\Theta_D,\mathbf{b}_{\text{cc},k},\mathbf{b}_{\text{cp},k}\}$.

I_s represents the swarm size, and I_f stands for the complexity in evaluating the fitness value in formulated optimization problems. Defining O_v as the size of optimization variables for formulated problems, we have $I_f \sim O_v^{3.5}$ [44], which is close to the per-iteration complexity of proposed method. In addition, the swarm size I_s and iteration number I_t increase with the search space dimension and problem complexity remarkably. Considering the high-dimensional optimization variables, the proposed method has lower computational complexity than the particle swarm optimization-based algorithms.

V. Extension to Non-linear Energy Harvesting

In above sections, we consider a scenario with classic linear energy harvesting model. In order to adjust the beamforming and reflecting optimization strategies to non-linear energy harvesters, we further consider the following non-linear energy harvesting model

$$P_k = \frac{\Psi_k - P_{\text{sat},k}\Delta_k}{1-\Delta_k}, \forall k \in \mathcal{K}, \tag{48}$$

where P_k denotes the power harvested by k-th IoT device, $\Delta_k = \frac{1}{1+\exp(a_k b_k)}$, $\Psi_k = \frac{P_{\text{sat},k}}{1+\exp(-a_k(P_{\text{EH},k}-b_k))}$, and $P_{\text{EH},k} = \|\mathbf{G}_{E,k}^H \mathbf{v}\|^2$. Noted that $P_{\text{sat},k}$ denotes the maximum harvested power at k-th IoT device, a_k and b_k are associated with circuit architecture. Therefore, the energy harvested by k-th IoT device is indicated as $E_k = T_{ET} P_k$.

In the MSE minimization problem and sum-rate maximization problem, the energy causality constraint is rewritten as

$$\|\mathbf{b}_{\text{cp},k}\|^2 + \|\mathbf{b}_{\text{cc},k}\|^2 \le \frac{T_{ET} P_k}{T_{IT}} + \frac{Q_{\text{ini},k}}{T_{IT}}, \forall k \in \mathcal{K}. \tag{49}$$

Similarly, the formulated MSE minimization problem and sum-rate maximization problem are strictly non-convex, which can be decoupled into several subproblems including receive beamforming optimization subproblem, phase shift optimization subproblem, and transmit beamforming optimization subproblem. Compared to the methods used in the scenario with linear energy harvesting model, we only need to make a simple modification for solving the decoupled subproblems in the scenario with non-linear energy harvesters. Specifically, the energy causality constraint in the receive beamforming optimization subproblem, phase shift optimization subproblem, and transmit beamforming optimization subproblem can be converted as

$$\|\mathbf{b}_{\text{cp},k}^*\|^2 + \|\mathbf{b}_{\text{cc},k}^*\|^2 \le \frac{T_{ET}}{T_{IT}} \frac{\Psi_k(\mathbf{v}, \mathbf{\Theta_E}^*) - P_{\text{sat},k}\Delta_k}{1-\Delta_k} + \frac{Q_{\text{ini},k}}{T_{IT}}, \forall k \in \mathcal{K}, \tag{50}$$

$$\|\mathbf{b}_{\text{cp},k}^*\|^2 + \|\mathbf{b}_{\text{cc},k}^*\|^2 \le \frac{T_{ET}}{T_{IT}} \frac{\Psi_k(\mathbf{v}^*, \mathbf{\Theta_E}) - P_{\text{sat},k}\Delta_k}{1-\Delta_k} + \frac{Q_{\text{ini},k}}{T_{IT}}, \forall k \in \mathcal{K}, \tag{51}$$

$$\|\mathbf{b}_{\text{cp},k}\|^2 + \|\mathbf{b}_{\text{cc},k}\|^2 \le \frac{T_{ET}}{T_{IT}} \frac{\Psi_k(\mathbf{v}^*, \mathbf{\Theta_E}^*) - P_{\text{sat},k}\Delta_k}{1-\Delta_k} + \frac{Q_{\text{ini},k}}{T_{IT}}, \forall k \in \mathcal{K}, \tag{52}$$

respectively. After some inequality transformations, (50)-(51) can be rewritten as

$$b_k - \frac{\ln\left(\frac{P_{\text{sat},k}}{P_{\text{sat},k}\Delta_k + \frac{T_{IT}}{T_{ET}}(\|\mathbf{b}_{\text{cp},k}^*\|^2 + \|\mathbf{b}_{\text{cc},k}^*\|^2 - \frac{Q_{\text{ini},k}}{T_{IT}})(1-\Delta_k)} - 1\right)}{a_k} \le \|(\mathbf{G}_{E,k}^*)^H \mathbf{v}\|^2, \forall k \in \mathcal{K}, \tag{53}$$

$$b_k - \frac{\ln\left(\frac{P_{\text{sat},k}}{P_{\text{sat},k}\Delta_k + \frac{T_{IT}}{T_{ET}}(\|\mathbf{b}_{\text{cp},k}^*\|^2 + \|\mathbf{b}_{\text{cc},k}^*\|^2 - \frac{Q_{\text{ini},k}}{T_{IT}})(1-\Delta_k)} - 1\right)}{a_k} \le \|\mathbf{G}_{E,k}^H \mathbf{v}^*\|^2, \forall k \in \mathcal{K}. \tag{54}$$

Since the right side of inequality (52) and the left side of inequalities (53)-(54) are constant in their corresponding subproblems, so the energy causality constraint in non-linear energy harvesting scenario is similar to that of linear energy harvesting scenario. As a result, the same variable substitution method at above sections can be exploited to transform (52)-(54) to the equivalent convex form. Therefore, the proposed joint beamforming and reflecting optimization methods can be directly utilized in the non-linear energy harvesting scenario after the simple modifications.

VI. Numerical Results

In this section, the performance of our proposed IRS-aided wireless powered AirComp and communication system is evaluated by numerical simulations. Moreover, the benchmark methods for comparison are listed as follows.

- *IRS with random phase:* In this strategy, the phase shift of reflection units is randomly selected from the interval $(0, 2\pi]$. Besides, the transmit and receive beamformers are jointly optimized to improve the computation or communication performance.
- *Without IRS:* In this strategy, no IRS is deployed in the wireless powered AirComp and communication network, and the transmit and receive beamforming will be jointly optimized to improve the computation accuracy or communication rate.
- *Computation only:* In this strategy, only the computation signals are transmitted from IoT devices to the BS, and the MSE is minimized by jointly optimizing the receive beamformer of BS, phase shifts of IRS, and transmit beamformers of IoT devices.
- *Communication only:* In this strategy, only the communication signals are transmitted from IoT devices to the BS, and the sum rate is maximized through jointly optimizing the receive beamformer of BS, phase shifts of IRS, and transmit beamformer of IoT devices.
- *Time-division computation and communication:* In this method, the uplink information transmissions and AirComp are conducted in a time-division manner with the aid of IRS.

In the simulations, the antennas of BS and IoT devices are set as $N_A = 10$ and $N_I = 4$, respectively, the number of reflection units and IoT devices are $M = 30$ and $K = 2$, respectively, the maximum transmit power of BS is set as

$P_{\max,A} = 20$ W, the initial energy of IoT devices is set as $Q_{\text{ini},k} = 0$ Joule, the noise power is $\delta^2 = 10^{-9}$ W, the time duration ratio between the energy transfer and uplink information transmission is set as $\frac{T_{ET}}{T_{IT}} = 1$, and the energy conversion efficiency is set as $\eta_k = 0.8$. Moreover, the BS, IRS, and IoT devices are located at [0 0 5], [0 5 3], ([2 7 0], [1 6 0]), respectively. The direct links between the BS and IoT devices are modeled as the Rayleigh fading channels, namely $\mathbf{G}_{d,k} = \sqrt{\gamma_1 d_{d,k}^{-\beta_1}}\hat{\mathbf{G}}_{d,k}$, where γ_1 denotes the channel gain at unit distance, $d_{d,k}$ is the distance between the BS and k-th IoT device, β_1 represents the path-loss factor, and $\hat{\mathbf{G}}_{d,k}$ follows complex Gaussian distribution with zero mean and unit variance. Moreover, the reflection channels follow the Rician fading model, which are expressed as

$$\mathbf{H} = \sqrt{\gamma_2 d_{r,0}^{-\beta_2}}\left(\sqrt{\frac{\kappa}{\kappa+1}}\mathbf{H}^{\text{LoS}} + \sqrt{\frac{1}{\kappa+1}}\mathbf{H}^{\text{NLoS}}\right), \quad (55)$$

$$\mathbf{G}_{r,k} = \sqrt{\gamma_3 d_{r,k}^{-\beta_3}}\left(\sqrt{\frac{\kappa}{\kappa+1}}\mathbf{G}_{r,k}^{\text{LoS}} + \sqrt{\frac{1}{\kappa+1}}\mathbf{G}_{r,k}^{\text{NLoS}}\right), \forall k \in \mathcal{K}, \quad (56)$$

where γ_i and β_i, $i \in \{2,3\}$, denote the channel gain at unit distance and the path-loss factor, respectively, κ is the Rician coefficient, $d_{r,0}$ stands for the distance between the BS and the IRS, $d_{r,k}$ represents the distance between the IRS and the k-th IoT device, $\mathbf{H}^{\text{LoS}}$ and $\mathbf{H}^{\text{NLoS}}$ indicate the line-of-sight (LoS) component and non-LoS component of $\mathbf{H}$, respectively, $\mathbf{G}_{r,k}^{\text{LoS}}$ and $\mathbf{G}_{r,k}^{\text{NLoS}}$ stand for the LoS component and non-LoS component of $\mathbf{G}_{r,k}$, respectively. Based on above simulation settings, our proposed methods are simulated by MATLAB R2012a, and the CVX toolbox is adopted as the convex optimization modeling system.

A. MSE of Computation Result

This subsection evaluates the MSE of computation result achieved by Algorithm 1. In this scenario, the simulation parameters are set as follows: $r_{\min,k} = 20$ dB, $\gamma_1 = \gamma_2 = \gamma_3 = 10^{-3}$, $\beta_1 = 3$, $\beta_2 = \beta_3 = 2.5$, $\kappa = 3$, $\chi_1 = 0.1$, and $\chi_2 = 0.01$.

Fig. 3 plots the MSE against the number of reflection elements at the IRS. As observed, the MSE realized by both the proposed method and the *computation only* method exhibits a decreasing trend with the increase of number of reflection elements at the IRS. Because that a larger number of reflection elements will provide higher degrees of freedom to align all the different IoT devices' channels. Moreover, we observe from this figure that our proposed method can obtain significantly lower MSE than both the *Without IRS* scheme and the *IRS with random phase* scheme, especially when the size of reflection units is large. In addition, the *computation only* scheme exhibits a slightly lower MSE than the proposed method. The reason is that the communication signal will incur the harmful co-channel interference to AirComp, and it will further lead to the increase of computation error, as shown in (7).

Fig. 4 shows the relationship between the MSE and the number of antennas at IoT devices. We observe from this figure that the MSE decreases with the increasing number of antennas at IoT devices. That is because that more refined transmit beamforming strategy will be designed to reduce the computation distortion, when each IoT device is equipped with a lager number of antennas. Moreover, due to the optimal configuration of IRS, the proposed method outperforms both the *IRS with random phase* scheme and the *Without IRS* scheme. Besides, when $N_I \geq 6$, the proposed method can achieve almost the same MSE of computation result, in comparison with the *computation only* scheme.

Fig. 5 evaluates the influence of maximum transmission power at the BS on the MSE achieved by Algorithm 1. As seen in this figure, the MSE decreases with the increase of maximum transmission power at the BS. Because that the IoT devices will harvest more energy to conduct efficient transmit beamforming to reduce the MSE. In addition, the proposed method is able to achieve at least 33% MSE reduction than both the *Without IRS* scheme and the *IRS with random phase* scheme. It further demonstrates that the optimal configuration of IRS phase shift is of great importance to reduce the computation error. Moreover, the proposed method will lead to at most 16% higher computation distortion than the *computation only* scheme.

B. Sum Rate of Information Transmissions

In this subsection, we show the sum rate achieved by Algorithm 2. In this scenario, the simulation parameters are set as follows: $\gamma_1 = \gamma_2 = \gamma_3 = 10^{-2}$, $\beta_1 = 2.5$, $\beta_2 = \beta_3 = 2$, $\kappa = 3$, and $\chi_3 = \chi_4 = \chi_5 = 1$.

Fig. 6 shows the curves of the sum rate against the number of reflection units at the IRS. One can observe that the sum rate increases with the number of reflection elements at the IRS. The reason is that a larger number of reflection elements contribute to more efficient reflect beamforming to alleviate the harmful interference between communication and computation signals. Besides, our proposed method outperforms the *IRS with random phase* scheme, and the performance gap increases with the size of reflection units at the IRS. It further verifies the necessity to optimize the IRS phase shift for improving the sum rate of considered systems. Moreover, it is found that the proposed method can realize a slightly lower sum rate than the *communication only* scheme. That is because the computation signal will lead to the increase of co-channel interference, and further reduces the SINR of information transmissions, as shown in (9).

Fig. 7 investigates the effect of the number of antennas at IoT devices on the sum rate achieved by Algorithm 2. As observed, the sum rate obtained by the proposed method increases with the number of antennas at IoT devices. That is because that more refined transmit beamforming will be designed to improve the sum rate with the increasing antennas of IoT devices. Moreover, the significant performance gain realized by the proposed method is demonstrated in this figure, as compared to the *IRS with random phase* scheme and the *time-division computation and communication* scheme. As expected, the IoT devices have to allocate the additional time to transmit the computation signals to the BS in the *time-division computation and communication* scheme, and it will lead to the reduction of available time for transmitting communication signals. Therefore, the proposed method

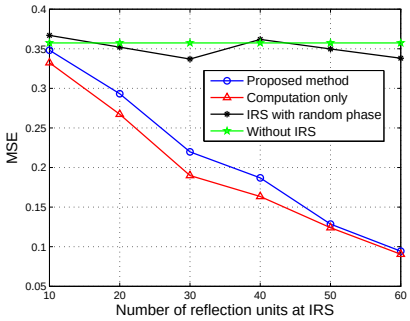

Fig. 3: MSE versus number of reflection units at IRS.

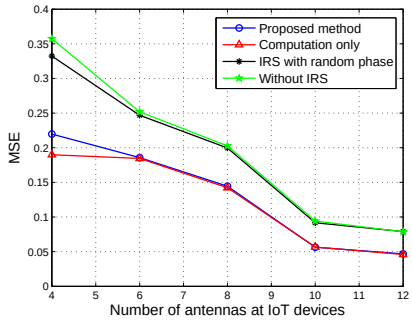

Fig. 4: MSE versus number of antennas at IoT devices.

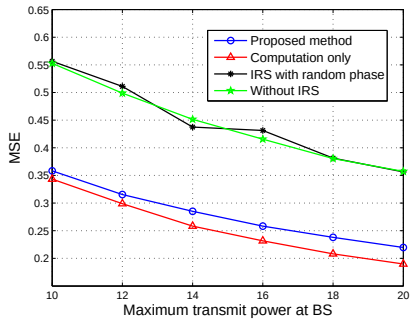

Fig. 5: MSE versus maximum transmit power at BS.

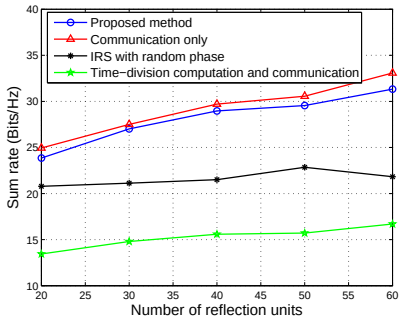

Fig. 6: Sum rate versus number of reflection units at IRS.

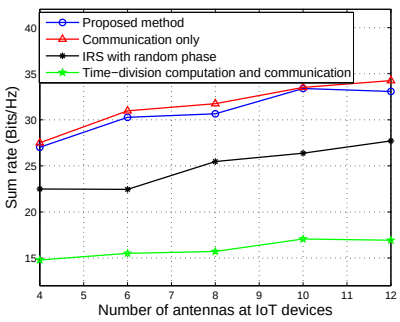

Fig. 7: Sum rate versus number of antennas at IoT devices.

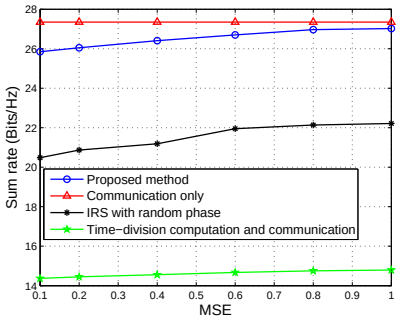

Fig. 8: Sum rate versus maximum tolerable MSE.

exhibits significantly higher sum-rate than the *time-division computation and communication* scheme.

Fig. 8 compares the proposed method with the considered benchmark methods under the varying maximum tolerable MSE $e_{\max}$. It is seen that the sum rate achieved by the proposed method increases with the growth of maximum tolerable MSE. Because that IoT devices can allocate more power for communication signals with the increase of $e_{\max}$, and it will further lead to the improvement of SINR of information transmissions. This figure further demonstrates the tradeoff between the achievable computation accuracy and communication rate for IRS-aided wireless powered AirComp and communication networks. Besides, the proposed method can realize at least 22% and 79% higher sum rate, in comparison with the *IRS with random phase* scheme and the *time-division computation and communication* scheme, respectively. In addition, it is found that the *communication only* scheme is superior to the proposed method in terms of sum rate, and the rate gain decreases with the growth of maximum tolerable MSE.

C. Convergence of proposed algorithms

Figs. 9-10 plot the convergence of proposed algorithms under different simulation parameters. It is seen from Fig. 9 that the MSE gradually decreases with the increase of iteration number, and then converges to a stationary point after no more than ten iterations. Meanwhile, we also observe from Fig. 10 that the sum rate will converge to the optimal solution after several iterations. Combined with the low per-iteration complexity, these simulation results reveal that proposed methods are computationally efficient.

VII. Conclusion

This paper proposed a novel framework for IRS-aided wireless powered AirComp and communication networks. In order to achieve accurate computations and high-speed communications, we developed two joint beamforming and reflection optimization algorithms for minimizing the computation error while ensuring the minimum SINR constraints, and maximizing the sum rate while guaranteeing the maximum computation error constraints, respectively. Simulation results showed that the proposed method realizes comparable computation accuracy and transmission rate than the *computation only* scheme and the *computation only* scheme, respectively. Moreover, the IRS-aided method is significantly superior to both the *without IRS* scheme and the *IRS with random phase* scheme in terms of MSE and sum rate.

In the future, this article can be extended to several interesting research directions. First, it is challenging and high-cost to obtain accurate channel state information for IRS-aided communication networks, especially when the IRS is equipped with massive reflection elements. Therefore, it is meaningful to investigate the robust beamforming and reflecting optimization strategy for IRS-aided wireless powered AirComp and communication networks considering imperfect channel state information. Second, the conventional reflecting-only IRS can only achieve the half-space coverage. Hence, the intelligent omni-surfaces can be exploited to achieve the full-space coverage for considered systems. Finally, this article

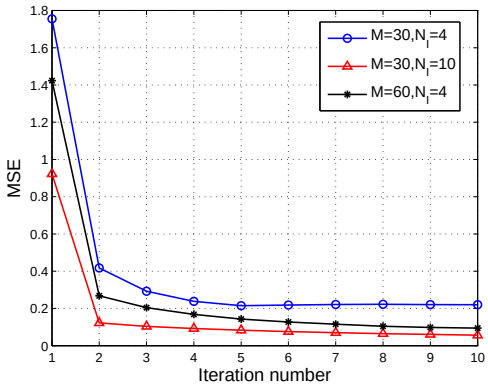

Fig. 9: Convergence of Algorithm 1.

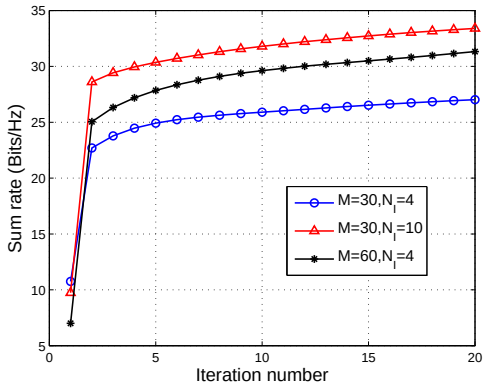

Fig. 10: Convergence of Algorithm 2.

adopted the ideal IRS phase shift model that cannot capture the phase-dependent amplitude variation at the IRS. Therefore, it is essential to adjust the beamforming and reflecting optimization scheme to practical IRS phase shift model.

REFERENCES

[1] A. Al-Fuqaha, M. Guizani, M. Mohammadi, M. Aledhari, and M. Ayyash, "Internet of things: A survey on enabling technologies, protocols, and applications," *IEEE Communications Surveys and Tutorials*, vol. 17, no. 4, pp. 2347–2376, 2015.

[2] B. Clerckx, R. Zhang, R. Schober, D. W. K. Ng, D. I. Kim, and H. V. Poor, "Fundamentals of wireless information and power transfer: From RF energy harvester models to signal and system designs," *IEEE Journal on Selected Areas in Communications*, vol. 37, no. 1, pp. 4–33, 2019.

[3] J. Hu, K. Yang, G. Wen, and L. Hanzo, "Integrated data and energy communication network: A comprehensive survey," *IEEE Communications Surveys and Tutorials*, vol. 20, no. 4, pp. 3169–3219, 2018.

[4] "Mi air charge technology," https://www.theverge.com/2021/1/28/22255625/xiaomi-mi-air-chargetechnology-wireless-charging.

[5] Z. Ding, X. Lei, G. K. Karagiannidis, R. Schober, J. Yuan, and V. K. Bhargava, "A survey on non-orthogonal multiple access for 5G networks: Research challenges and future trends," *IEEE Journal on Selected Areas in Communications*, vol. 35, no. 10, pp. 2181–2195, 2017.

[6] Y. Liu, S. Zhang, X. Mu, Z. Ding, R. Schober, N. Al-Dhahir, E. Hossain, and X. Shen, "Evolution of noma toward next generation multiple access (NGMA) for 6G," *IEEE Journal on Selected Areas in Communications*, vol. 40, no. 4, pp. 1037–1071, 2022.

[7] Z. Ding, Y. Liu, J. Choi, Q. Sun, M. Elkashlan, I. Chih-Lin, and H. V. Poor, "Application of non-orthogonal multiple access in lte and 5G networks," *IEEE Communications Magazine*, vol. 55, no. 2, pp. 185–191, 2017.

[8] F. Zhou, Y. Wu, R. Q. Hu, Y. Wang, and K. K. Wong, "Energy-efficient NOMA enabled heterogeneous cloud radio access networks," *IEEE Network*, vol. 32, no. 2, pp. 152–160, 2018.

[9] A. Ihsan, W. Chen, M. Asif, W. U. Khan, Q. Wu, and J. Li, "Energy-efficient IRS-aided NOMA beamforming for 6G wireless communications," *IEEE Transactions on Green Communications and Networking*, vol. 6, no. 4, pp. 1945–1956, 2022.

[10] B. Nazer and M. Gastpar, "Computation over multiple-access channels," *IEEE Transactions on information theory*, vol. 53, no. 10, pp. 3498–3516, 2007.

[11] L. Chen, N. Zhao, Y. Chen, F. R. Yu, and G. Wei, "Over-the-air computation for IoT networks: Computing multiple functions with antenna arrays," *IEEE Internet of Things Journal*, vol. 5, no. 6, pp. 5296–5306, 2018.

[12] G. Zhu and K. Huang, "MIMO over-the-air computation for high-mobility multimodal sensing," *IEEE Internet of Things Journal*, vol. 6, no. 4, pp. 6089–6103, 2019.

[13] L. Chen, N. Zhao, Y. Chen, F. R. Yu, and G. Wei, "Over-the-air computation for cooperative wideband spectrum sensing and performance analysis," *IEEE Transactions on Vehicular Technology*, vol. 67, no. 11, pp. 10 603–10 614, 2018.

[14] J. Zheng, H. Tian, W. Ni, W. Ni, and P. Zhang, "Balancing accuracy and integrity for reconfigurable intelligent surface-aided over-the-air federated learning," *IEEE Transactions on Wireless Communications*, vol. 21, no. 12, pp. 10 964–10 980, 2022.

[15] S. Mao, N. Zhang, J. Hu, and K. Yang, "Intelligent reflecting surface-assisted over-the-air computation for backscatter sensor networks," *IEEE Transactions on Vehicular Technology*, vol. 72, no. 5, pp. 6839–6843, 2023.

[16] W. Liu, X. Zang, Y. Li, and B. Vucetic, "Over-the-air computation systems: Optimization, analysis and scaling laws," *IEEE Transactions on Wireless Communications*, vol. 19, no. 8, pp. 5488–5502, 2020.

[17] X. Cao, G. Zhu, J. Xu, and K. Huang, "Cooperative interference management for over-the-air computation networks," *IEEE Transactions on Wireless Communications*, vol. 20, no. 4, pp. 2634–2651, 2021.

[18] M. Fu, Y. Zhou, Y. Shi, W. Chen, and R. Zhang, "UAV aided over-the-air computation," *IEEE Transactions on Wireless Communications*, vol. 21, no. 7, pp. 4909–4924, 2022.

[19] X. Li, G. Zhu, Y. Gong, and K. Huang, "Wirelessly powered data aggregation for IoT via over-the-air function computation: Beamforming and power control," *IEEE Transactions on Wireless Communications*, vol. 18, no. 7, pp. 3437–3452, Jul. 2019.

[20] Q. Qi, X. Chen, C. Zhong, and Z. Zhang, "Integrated sensing, computation and communication in B5G cellular internet of things," *IEEE Transactions on Wireless Communications*, vol. 20, no. 1, pp. 332–344, 2021.

[21] ——, "Integration of energy, computation and communication in 6G cellular internet of things," *IEEE Communications Letters*, vol. 24, no. 6, pp. 1333–1337, 2020.

[22] Q. Wu, S. Zhang, B. Zheng, C. You, and R. Zhang, "Intelligent reflecting surface-aided wireless communications: A tutorial," *IEEE Transactions on Communications*, vol. 69, no. 5, pp. 3313–3351, 2021.

[23] C. Huang, A. Zappone, G. C. Alexandropoulos, M. Debbah, and C. Yuen, "Reconfigurable intelligent surfaces for energy efficiency in wireless communication," *IEEE Transactions on Wireless Communications*, vol. 18, no. 8, pp. 4157–4170, 2019.

[24] Y. Liu, X. Liu, X. Mu, T. Hou, J. Xu, M. Di Renzo, and N. Al-Dhahir, "Reconfigurable intelligent surfaces: Principles and opportunities," *IEEE Communications Surveys and Tutorials*, vol. 23, no. 3, pp. 1546–1577, 2021.

[25] S. Mao, N. Zhang, L. Liu, J. Wu, M. Dong, K. Ota, T. Liu, and D. Wu, "Computation rate maximization for intelligent reflecting surface enhanced wireless powered mobile edge computing networks," *IEEE Transactions on Vehicular Technology*, vol. 70, no. 10, pp. 10 820–10 831, Oct. 2021.

[26] C. Pan, H. Ren, K. Wang, M. Elkashlan, A. Nallanathan, J. Wang, and L. Hanzo, "Intelligent reflecting surface aided MIMO broadcasting for simultaneous wireless information and power transfer," *IEEE Journal on Selected Areas in Communications*, vol. 38, no. 8, pp. 1719–1734, 2020.

[27] B. Lyu, P. Ramezani, D. T. Hoang, and A. Jamalipour, "IRS-assisted downlink and uplink NOMA in wireless powered communication networks," *IEEE Transactions on Vehicular Technology*, vol. 71, no. 1, pp. 1083–1088, 2022.

[28] Q. Wu and R. Zhang, "Joint active and passive beamforming optimization for intelligent reflecting surface assisted SWIPT under QoS

constraints," *IEEE Journal on Selected Areas in Communications*, vol. 38, no. 8, pp. 1735–1748, Aug. 2020.
[29] Z. Li, W. Chen, Q. Wu, H. Cao, K. Wang, and J. Li, "Robust beamforming design and time allocation for IRS-assisted wireless powered communication networks," *IEEE Transactions on Communications*, vol. 70, no. 4, pp. 2838–2852, 2022.
[30] Y. Zheng, S. Bi, Y. J. Zhang, Z. Quan, and H. Wang, "Intelligent reflecting surface enhanced user cooperation in wireless powered communication networks," *IEEE Wireless Communications Letters*, vol. 9, no. 6, pp. 901–905, 2020.
[31] W. Shi, Q. Wu, F. Xiao, F. Shu, and J. Wang, "Secrecy throughput maximization for IRS-aided MIMO wireless powered communication networks," *IEEE Transactions on Communications*, vol. 70, no. 11, pp. 7520–7535, 2022.
[32] S. Mao, L. Liu, and C. Shao, "Energy-efficient scheduling for active RIS-assisted self-sustainable wireless powered IoT networks in smart societies," *Sustainable Cities and Society*, vol. 95, p. 104559, 2023.
[33] S. Mao, L. Liu, N. Zhang, J. Hu, K. Yang, M. Dong, and K. Ota, "Resource scheduling for intelligent reflecting surface-assisted full-duplex wireless-powered communication networks with phase errors," *IEEE Internet of Things Journal*, vol. 10, no. 7, pp. 6018–6030, 2023.
[34] W. Fang, Y. Jiang, Y. Shi, Y. Zhou, W. Chen, and K. B. Letaief, "Over-the-air computation via reconfigurable intelligent surface," *IEEE Transactions on Communications*, vol. 69, no. 12, pp. 8612–8626, 2021.
[35] X. Zhai, G. Han, Y. Cai, Y. Liu, and L. Hanzo, "Simultaneously transmitting and reflecting (STAR) RIS assisted over-the-air computation systems," *IEEE Transactions on Communications*, vol. 71, no. 3, pp. 1309–1322, 2023.
[36] X. Zhai, G. Han, Y. Cai, and L. Hanzo, "Joint beamforming aided over-the-air computation systems relying on both BS-side and user-side reconfigurable intelligent surfaces," *IEEE Transactions on Wireless Communications*, vol. 21, no. 12, pp. 10 766–10 779, 2022.
[37] ——, "Beamforming design based on two-stage stochastic optimization for RIS-assisted over-the-air computation systems," *IEEE Internet of Things Journal*, vol. 9, no. 7, pp. 5474–5488, 2022.
[38] Z. Wang, Y. Shi, Y. Zhou, H. Zhou, and N. Zhang, "Wireless-powered over-the-air computation in intelligent reflecting surface-aided IoT networks," *IEEE Internet of Things Journal*, vol. 8, no. 3, pp. 1585–1598, Feb. 2021.
[39] S. Mao, S. Leng, S. Maharjan, and Y. Zhang, "Energy efficiency and delay tradeoff for wireless powered mobile-edge computing systems with multi-access schemes," *IEEE Transactions on Wireless Communications*, vol. 19, no. 3, pp. 1855–1867, 2020.
[40] B. Zheng, C. You, W. Mei, and R. Zhang, "A survey on channel estimation and practical passive beamforming design for intelligent reflecting surface aided wireless communications," *IEEE Communications Surveys and Tutorials*, vol. 24, no. 2, pp. 1035–1071, 2022.
[41] M. Grant and S. Boyd, "CVX: Matlab software for disciplined convex programming, version 2.1," 2014.
[42] L. Zhu, J. Zhang, Z. Xiao, X. Cao, D. O. Wu, and X.-G. Xia, "Joint Tx-Rx beamforming and power allocation for 5G millimeter-wave non-orthogonal multiple access networks," *IEEE Transactions on Communications*, vol. 67, no. 7, pp. 5114–5125, 2019.
[43] Y. Cao, T. Lv, and W. Ni, "Two-timescale optimization for intelligent reflecting surface-assisted MIMO transmission in fast-changing channels," *IEEE Transactions on Wireless Communications*, vol. 21, no. 12, pp. 10 424–10 437, 2022.
[44] H. Zhang, Y. Huang, C. Li, and L. Yang, "Secure beamforming design for SWIPT in MISO broadcast channel with confidential messages and external eavesdroppers," *IEEE Transactions on Wireless Communications*, vol. 15, no. 11, pp. 7807–7819, 2016.